Calcium Coding and Adaptive Temporal Computation in Cortical Pyramidal Neurons

XIAO-JING WANG
Center for Complex Systems and Department of Physics, Brandeis University, Waltham, Massachusetts 02254

Wang, Xiao-Jing. Calcium coding and adaptive temporal computation in cortical pyramidal neurons. *J. Neurophysiol.* 79: 1549–1566, 1998. In this work, we present a quantitative theory of temporal spike-frequency adaptation in cortical pyramidal cells. Our model pyramidal neuron has two-compartments (a ''soma'' and a ''dendrite'') with a voltage-gated Ca^{2+} conductance (g_{Ca}) and a Ca^{2+}-dependent K^+ conductance (g_{AHP}) located at the dendrite or at both compartments. Its frequency-current relations are comparable with data from cortical pyramidal cells, and the properties of spike-evoked intracellular $[Ca^{2+}]$ transients are matched with recent dendritic $[Ca^{2+}]$ imaging measurements. Spike-frequency adaptation in response to a current pulse is characterized by an adaptation time constant τ_{adap} and percentage adaptation of spike frequency F_{adap} [% (peak − steady state)/peak]. We show how τ_{adap} and F_{adap} can be derived in terms of the biophysical parameters of the neural membrane and $[Ca^{2+}]$ dynamics. Two simple, experimentally testable, relations between τ_{adap} and F_{adap} are predicted. The dependence of τ_{adap} and F_{adap} on current pulse intensity, electrotonic coupling between the two compartments, g_{AHP} as well the $[Ca^{2+}]$ decay time constant τ_{Ca}, is assessed quantitatively. In addition, we demonstrate that the intracellular $[Ca^{2+}]$ signal can encode the instantaneous neuronal firing rate and that the conductance-based model can be reduced to a simple calcium-model of neuronal activity that faithfully predicts the neuronal firing output even when the input varies relatively rapidly in time (tens to hundreds of milliseconds). Extensive simulations have been carried out for the model neuron with random excitatory synaptic inputs mimicked by a Poisson process. Our findings include *1*) the instantaneous firing frequency (averaged over trials) shows strong adaptation similar to the case with current pulses; *2*) when the g_{AHP} is blocked, the dendritic g_{Ca} could produce a hysteresis phenomenon where the neuron is driven to switch randomly between a quiescent state and a repetitive firing state. The firing pattern is very irregular with a large *coefficient of variation* of the interspike intervals (ISI CV > 1). The ISI distribution shows a long tail but is not bimodal. *3*) By contrast, in an intrinsically bursting regime (with different parameter values), the model neuron displays a random temporal mixture of single action potentials and brief bursts of spikes. Its ISI distribution is often bimodal and its power spectrum has a peak. *4*) The spike-adapting current I_{AHP}, as delayed inhibition through intracellular Ca^{2+} accumulation, generates a ''forward masking'' effect, where a masking input dramatically reduces or completely suppresses the neuronal response to a subsequent test input. When two inputs are presented repetitively in time, this mechanism greatly enhances the ratio of the responses to the stronger and weaker inputs, fulfilling a cellular form of lateral inhibition in time. *5*) The $[Ca^{2+}]$-dependent I_{AHP} provides a mechanism by which the neuron unceasingly adapts to the stochastic synaptic inputs, even in the stationary state following the input onset. This creates strong negative correlations between output ISIs in a frequency-dependent manner, while the Poisson input is totally uncorrelated in time. Possible functional implications of these results are discussed.

INTRODUCTION

Cortical neurons display a large repertoire of voltage- and calcium-gated potassium ion channels with kinetic time constants ranging from milliseconds to seconds (Llinás 1988; Rudy 1988; Storm 1990). The diversity and richness of K^+ conductances indicate that they likely contribute to neuronal input-output computation in ways more complex than sculpturing the waveform of action potentials or regulating the overall membrane excitability. For example, slow K^+ currents, in interplay with Ca^{2+} and/or Na^+ currents, can generate rhythmic firing patterns intrinsic to single neurons (Llinás 1988; Wang and Rinzel 1995). Or a slowly inactivating K^+ current can integrate synaptic inputs in a temporal-history–dependent manner (Storm 1988; Turrigiano et al. 1996; Wang 1993). Moreover, K^+ channels at dendritic sites are capable of modifying cable properties and may regulate synaptic transmission (Hoffman et al. 1997) and prevent input saturation (Bernander et al. 1994; Wilson 1995).

Spike-frequency adaptation that depends on a Ca^{2+}-gated K^+ conductance is a conspicuous neuronal firing characteristic exhibited by a majority of (''regular spiking'') pyramidal neurons in neocortex and hippocampus (Avoli et al. 1994; Connors et al. 1982; Foehring et al. 1991; Gustafsson and Wigström 1981; Lanthorn et al. 1984; Lorenzon and Foehring 1992; Mason and Larkman 1990; McCormick et al. 1985). In response to a constant current pulse, the firing frequency of an adapting neuron is initially high then decreases to a lower steady-state plateau level within hundreds of milliseconds. This phenomenon has been studied intensively in in vitro slice experiments (as is the case for all afore-cited references). Recently, Ahmed et al. (1993; B. Ahmed, C. Anderson, R. J. Douglas; K.A.C. Martin, unpublished results) observed and quantified spike-frequency adaptation of in vivo cortical neurons with intracellular recordings from the primary visual cortex of the anesthetized cat. They found that when subjected to a injected current pulse, the adaptation time course of cortical cells can be fitted empirically by an exponential time course (Ahmed et al. 1993; unpublished results), i.e., the instantaneous firing rate $f(t) = f_{ss} + (f_0 - f_{ss}) \exp(-t/\tau_{adap})$, where f_0 is the initial firing rate, f_{ss} is the steady-state firing rate, and τ_{adap} is an *adaptation time constant.* Thus this time course is characterized by two quantities: τ_{adap} and the percentage adaptation of firing frequency $F_{adap} = (f_0 - f_{ss})/f_0$. Ahmed

et al. (1993; unpublished results) found that $\tau_{adap} = 10-50$ ms and $F_{adap} = 50-70\%$ with a significant difference between superficial and deep layer neurons. They also performed computer simulations that reproduced many of their observations.

In this modeling work, we present a quantitative study of spike-frequency adaptation temporal dynamics, which, in particular, yields analytical expressions for τ_{adap} and F_{adap} in terms of the cellular biophysical parameters. We also explore possible implications of this phenomenon in the real-time input-output computation of cortical neurons. Compared with an early quantitative work modeling spike-frequency adaptation in motoneurons by Baldsissera and Gustafsson (1974), the present study benefitted from a number of recent experimental findings and quantitative data about the cellular mechanisms underlying the spike-frequency adaptation phenomenon. First, it is well known that the spike-frequency adaptation is produced mainly by a voltage-independent, Ca^{2+}-dependent K^+ current, although other K^+ currents (such as the M current) also are involved to a lesser degree (Madison and Nicoll 1984; Madison et al. 1987; McCormick and Williamson 1989). This current is associated with the slow after hyperpolarization (AHP) after a burst of spikes, hence is called the AHP current (I_{AHP}) (Hotson and Prince 1980; Lancaster and Adams 1986; Schwindt et al. 1988). Second, it has been demonstrated by photolytic manipulation of Ca^{2+} that the intrinsic gating of I_{AHP} is rapid; its slow activation is thus attributable to the kinetics of the cytoplasmic calcium concentration $[Ca^{2+}]$ (Lancaster and Zucker 1994). Third, spike-evoked $[Ca^{2+}]$ transients now can be measured by fluorescence imaging techniques (see Yuste and Tank 1996 for a review). Recently, to overcome the problem that a $[Ca^{2+}]$ indicator dye like Fura-2 is also a $[Ca^{2+}]$ buffer, Helmchen et al. (1996) used increasingly low concentrations of Fura-2 and, by extrapolation to zero dye concentration, obtained measurements of putatively intrinsic $[Ca^{2+}]$ transient signals. Their estimated spike-evoked $[Ca^{2+}]$ transient from dendrites of cortical pyramidal neurons are larger and faster than previously reported. In the model pyramidal neuron of the present paper, the calcium dynamics (spike-evoked influx and decay) is constrained by accurate measurements of Helmchen et al. (1996).

Can calcium signaling perform interesting sensory computation in cortical neurons? In previous computational models, spike-frequency adaptation has been incorporated as a gain control mechanism for neuronal excitability (Barkai and Hasselmo 1994; Douglas et al. 1995). However, the adaptation temporal dynamics, i.e., its role in moment-to-moment neural computation in response to time-varying inputs, has not been emphasized. Through spike-frequency adaptation, $[Ca^{2+}]$ dynamics produces a ''forward masking'' phenomenon: the neuronal response to a stimulus may be masked due to another stimulus that precedes it in time as was demonstrated experimentally in the cricket auditory neurons (Sobel and Tank 1994). Results reported here suggest that such an effect also exists in cortical pyramidal cells and may be used to selectively respond to temporal input patterns. In particular, when two or several competing inputs are presented, the neuronal output is sharply ''tuned'' to the strongest input, and the responses to weaker inputs are greatly suppressed. Furthermore, if the input consists of temporally uncorrelated excitatory postsynaptic potentials (EPSPs) (a Poisson process), spike-frequency adaptation leads to strong anticorrelation between the consecutive interspike intervals of the output spike train. These results indicate that the adaptation mechanism is operative even in the stationary state after the input onset, and suggest a direct means to assess its efficacy from extracellularly recorded spike trains.

METHODS

Model

The neuron model has two compartments, representing the dendrite and the soma plus axonal initial segment, respectively (Pinsky and Rinzel 1994). Many of our results can be obtained with a single compartment. However, we used a two-compartment model for three reasons. *1*) Ca^{2+} imaging measurements from pyramidal cells show spike-evoked $[Ca^{2+}]$ transient that is much larger at the dendrite than at the soma (Jaffe et al. 1994; Schiller et al. 1995; Svoboda et al. 1997; Yuste et al. 1994), and the $[Ca^{2+}]$ influx is produced primarily by Ca^{2+} entry through voltage-gated channels (Miyakawa et al. 1992). In the present model, we focus mainly on spike-frequency adaptation that is caused by a dendritic $[Ca^{2+}]$-dependent I_{AHP}. *2*) We wanted to see whether our theoretical analysis can be carried out even with two (or more) compartments. When I_{AHP} is present both at soma and dendrite, we show that there are two ''calcium modes'' and the spike-frequency adaptation time course should be described as a sum of two exponentials. And *3*) with an appropriate choice of parameters, the neuron model displays burst firing patterns that require weak electrotonic interactions between the two compartments.

The dendritic compartment has a high-threshold calcium current (L type), I_{Ca}, and a calcium-dependent potassium current I_{AHP}. The somatic compartment contains spike generating currents (I_{Na} and I_K) and possibly also I_{Ca} and I_{AHP}. The somatic and dendritic membrane potentials V_s and V_d obey the following current-balance equations

$$C_m \frac{dV_s}{dt} = -I_L - I_{Na} - I_K - I_{Ca} - I_{AHP} - \frac{g_c}{p}(V_s - V_d) + I \qquad (1)$$

$$C_m \frac{dV_d}{dt} = -I_L - I_{Ca} - I_{AHP} - \frac{g_c}{(1-p)}(V_d - V_s) - I_{syn} \qquad (2)$$

where $C_m = 1\ \mu F/cm^2$ and $I_L = g_L(V - V_L)$ is the leak current. Following Pinsky and Rinzel (1994), we express the current flows between the soma and dendrite [proportional to $(V_s - V_d)$] in microamperes per square centimeter, with the coupling conductance $g_c = 2\ mS/cm^2$, and the parameter p = somatic area/total area = 0.5. Other, voltage-gated currents are described below. The cell is either excited by an injected current I (in $\mu A/cm^2$) to the soma or by a random synaptic input I_{syn} of the α-amino-3-hydroxy-5-methyl-4-isoxazolepropionic acid type to the dendrite. $I_{syn} = g_{syn}\, s(V - E_{syn})$; the gating variable s obeys the equation $ds/dt = \eta(t) - s/\tau_s$, where $\eta(t)$ is a Poisson point-process with a rate λ, $E_{syn} = 0$ mV, $\tau_s = 0.5$ ms, and $g_{syn} = 0.08\ mS/cm^2$ (if present).

The voltage-dependent currents are described by the Hodgkin-Huxley formalism (Hodgkin and Huxley 1952). Thus a gating variable x satisfies a first-order kinetics

$$\frac{dx}{dt} = \phi_x[\alpha_x(V)(1 - x) - \beta_x(V)x] = \phi_x[x_\infty(V) - x]/\tau_x(V) \qquad (3)$$

The sodium current $I_{Na} = g_{Na} m_\infty^3(V) h(V - V_{Na})$, where the fast activation variable is replaced by its steady state, $m_\infty = \alpha_m/(\alpha_m + \beta_m)$, $\alpha_m = -0.1(V + 33)/\{\exp[-0.1(V + 33)] - 1\}$, $\beta_m =$

4 $\exp[-(V + 58)/12]$, $\alpha_h = 0.07 \exp[-(V + 50)/10]$, and $\beta_h = 1/\{\exp[-0.1(V + 20)] + 1\}$. The delayed rectifier $I_K = g_K n^4 (V - V_K)$, where $\alpha_n = -0.01(V + 34)/\{\exp[-0.1(V + 34)] - 1\}$, and $\beta_n = 0.125 \exp[-(V + 44)/25]$. The temperature factor $\phi_h = \phi_n = 4$.

The high-threshold calcium current $I_{Ca} = g_{Ca} m_\infty (V - V_{Ca})$, where m is replaced by its steady-state $m_\infty(V) = 1/\{1 + \exp[-(V + 20)]/9\}$ (Kay and Wong 1987). The voltage-independent, calcium-activated potassium current $I_{AHP} = g_{AHP}[[Ca^{2+}]/([Ca^{2+}] + K_D)](V - V_K)$, with $K_D = 30$ μM. The intracellular calcium concentration $[Ca^{2+}]$ is assumed to be governed by a leaky-integrator (Helmchen et al. 1996; Tank et al. 1995; Traub 1982)

$$\frac{d[Ca^{2+}]}{dt} = -\alpha I_{Ca} - [Ca^{2+}]/\tau_{Ca} \quad (4)$$

where α is proportional to S/V with S being the membrane area and V the volume immediately beneath the membrane (Yamada et al. 1989). We used $\alpha = 0.002$ [in μM (ms μA)$^{-1}$cm^2] so that the $[Ca^{2+}]$ influx per spike is ~200 nM (Helmchen et al. 1996). The various extrusion and buffering mechanisms are described collectively by a first-order decay process with a time constant $\tau_{Ca} = 80$ ms (Helmchen et al. 1996; Markram et al. 1995; Svoboda et al. 1997).

The parameter values for the spike-generating currents and the I_{AHP} were chosen so that the model displayed the initial as well as the adapted *f-I* curves similar to the data of McCormick et al. (1985) and Mason and Larkman (1990): $g_L = 0.1$, $g_{Na} = 45$, $g_K = 18$, dendritic $g_{Ca} = 1$, and $g_{AHP} = 5$ (in mS/cm^2); $V_L = -65$, $V_{Na} = +55$, $V_K = -80$, $V_{Ca} = +120$ (in mV). The somatic g_{Ca} and g_{AHP} are zero except for Fig. 7. The resting state (with $I = 0$ and $g_{syn} = 0$) is at $V_s = -64.8$ and $V_d = -64$ mV.

The model was simulated on a Silicon Graphics Workstation, using a fourth-order Runge-Kutta method, with time step dt = 0.02–0.05 ms.

Statistical analysis

With Poisson synaptic inputs, each random output train of spike times is converted into a sequence of interspike intervals $\{t_1, t_2, t_3, \ldots, t_N\}$. The interspike interval (ISI) histogram is tabulated, with a mean μ and a standard deviation σ given by

$$\mu = \frac{1}{N}\sum_{n=1}^{N} t_n; \quad \sigma = \sqrt{\frac{1}{N}\sum_{n=1}^{N}(t_n - \mu)^2}$$

The ISI variability is quantified by the *coefficient of variation* (CV) (Softky and Koch 1993; Tuckwell 1988)

$$CV = \sigma/\mu \quad (6)$$

The statistical interdependence between consecutive ISIs is measured by the *coefficient of correlation* (CC) (Perkel et al. 1967; Tuckwell 1988)

$$CC = \frac{\langle (t_{n+1} - \mu)(t_n - \mu)\rangle}{\sigma^2} = \frac{\frac{1}{N-1}\sum_{n=1}^{N-1}(t_{n+1} - \mu)(t_n - \mu)}{\sigma^2} \quad (7)$$

which is between −1 and +1. The CC can be interpreted as follows. Suppose that we have an ISI *return map*, where t_{n+1} is plotted against t_n. To assess how ISIs (t_{n+1}) depend on their preceding values (t_n), we calculate the *conditional average of* t_{n+1} for each given t_n, $\langle t_{n+1} | t_n \rangle$. If this function of t_n is linear, then its slope is the same as the CC (see APPENDIX A for a derivation of this statement).

The temporal correlations are further assessed by the power spectrum of the spike train (with a time bin of 1 ms), using the subroutine Spctrm.c from Numerical Recipes (Press et al. 1989), modified by Yinghui Liu.

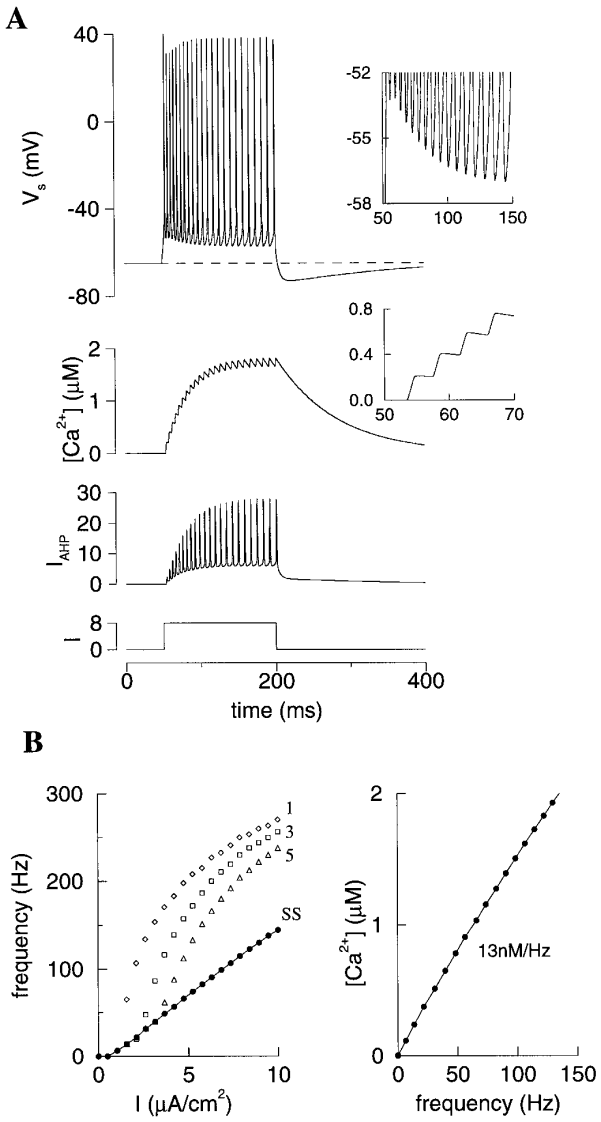

FIG. 1. Spike-frequency adaptation characteristics. *A*: an example of spike-frequency adaptation in response to a current pulse. Adaptation is accompanied by a gradual increase of the fast spike afterhyperpolarization (AHP; *top, inset*). Each action potential generates a $[Ca^{2+}]$ influx of ~200 nM (*bottom, inset*), and the adaptation time course follows that of $[Ca^{2+}]$ (hence I_{AHP}) accumulation. Slow AHP after the spike firing mirrors the $[Ca^{2+}]$ decay process. *B*: 1st, 3rd, and 5th instantaneous firing rates and the steady-state firing rate vs. the applied current intensity (*left*). Initial *f-I* curves are nonlinear, but the steady-state *f-I* relation is essentially linear. Plateau $[Ca^{2+}]$ level is a linear function of the steady-state firing rate, with a slope of ~13 nM/Hz (*right*).

RESULTS

Time course of spike-frequency adaptation

In response to a depolarizing current pulse, the model neuron initially fires at a high frequency, then adapts to a lower steady-state frequency (Fig. 1*A*). Spike-frequency adaptation is accompanied by a gradual increase of the fast spike AHP (from −53 to −57 mV, see Fig. 1*A*, *inset*). This

firing pattern is in parallel with the time course of Ca^{2+} accumulation, at a rate of ≃200 nM/spike [comparable with the $[Ca^{2+}]$ imaging measurements from proximal apical dendrites of cortical layer V pyramidal cells (Helmchen et al. 1996)]. The I_{AHP} increases with $[Ca^{2+}]$, hence the cell is gradually hyperpolarized and the firing frequency is decreased in time. In the steady state, an equilibrium is reached in the $[Ca^{2+}]$ dynamics, when the spike-evoked $[Ca^{2+}]$ influx rate is balanced with the $[Ca^{2+}]$ decay rate. After the current pulse, there is a long-lasting AHP that mirrors the Ca^{2+} (hence the I_{AHP}) decay (Fig. 1*A*).

Frequency-current *f-I* curves are shown in Fig. 1*B* (*left*), for the initial first, third, and fifth interspike intervals, as well as the steady state. At the onset of repetitive firing (rheobase I ≃ 0.5), the firing frequency starts at zero, through a homoclinic bifurcation of the saddle-node type (see also Crook et al. 1997). It is noticeable that the initial *f-I* curves are quite nonlinear, but the steady-state *f-I* relation is very close to linear, similar to regular spiking pyramidal neurons (cf. Figs. 8–9 in Mason and Larkman 1990). Intuitively, the adapting AHP-current provides a delayed negative feedback to the cell. It is larger at higher firing frequencies, thus the difference between the initial f_0 and the final f_{ss} increases with the current intensity. As a result, the steady-state input-output relation is linearized by the I_{AHP}. We also computed the mean dendritic $[Ca^{2+}]$ as I was varied. Its steady-state plateau level depends linearly on f_{ss} (Fig. 1*B*, *right*), with a slope ≃ 17 nM/Hz (compared with the measured 16 nM/Hz from dendrites of layer V pyramidal cells) (Helmchen et al. 1996). In this sense, the dendritic Ca^{2+} level encodes the neuronal firing activity (Helmchen et al. 1996; Johnston 1996).

For the spike train in Fig. 1, the instantaneous firing rate $f(t)$ is defined as the reciprocal of ISIs (Fig. 2*A*, *top*). Its time course can be well fitted by a mono-exponential curve, $f(t) = A + B\exp(-t/\tau_{adap})$, where $A = f_{ss}$, and $B = f_0 - f_{ss}$. The empirical best fit is given by $f(t) = 116 + 156\exp(-t/33)$. Thus $\tau_{adap} = 33$ ms, and the percentage adaptation $F_{adap} = (f_0 - f_{ss})/f_0 = B/(A + B) = 57\%$. The $[Ca^{2+}]$ also follows an exponential time course with the same time constant τ_{adap}, the steady-state plateau is $[Ca^{2+}]_{ss} = 1.74$ μM. Note that τ_{adap} is much shorter than the decay time constant $\tau_{Ca} = 80$ ms. We now show how this adaptation time course, given a constant current pulse, can be predicted quantitatively from the biophysics of the membrane dynamics *Eqs. 1–4*. We shall see further that this description leads to a calcium-coding model of neuronal output, even when the input varies temporally.

The fast-slow variable dissection method (Baer et al. 1995; Ermentrout 1994; Guckenheimer et al. 1997; Rinzel 1987; Wang and Rinzel 1995) is based on the observation that Ca^{2+} evolves much more slowly than the membrane potential and the other channel gating variables of the model and that this slow $[Ca^{2+}](t)$ determines the adaptation time course. Thus we can first analyze the fast subsystem and the slow $[Ca^{2+}]$ dynamics separately then put them back together. This is done in three steps (see APPENDIX B for details). In *step 1*, the fast electrical subsystem is analyzed while considering the slow $[Ca^{2+}]$ as if it was a static parameter rather than a dynamical variable. This allows us to determine the *functional* $[Ca^{2+}]$ dependence of the firing frequency $f([Ca^{2+}])$ as well as other voltage-dependent quantities like $\langle I_{Ca}\rangle$, where $\langle x\rangle$ denotes an average of x over a typical ISI. The functional $[Ca^{2+}]$ dependence of $f([Ca^{2+}])$ and of $\langle I_{Ca}\rangle$ was found to be approximately linear (Figs. 2, *B* and *C*)

$$f \simeq f_0 - G_f[Ca^{2+}]; \quad \langle I_{CA}\rangle \simeq \langle I_{Ca}\rangle_0 + G_{cc}[Ca^{2+}] \qquad (8)$$

where $f_0 = 271$ Hz is the initial firing frequency, and $G_f = -df/d[Ca^{2+}] = 84$ (in Hz/μM) is a negative-feedback "gain parameter" for the firing frequency. $\langle I_{Ca}\rangle_0 = -28.8$ μA/cm^2 is the initial $\langle I_{Ca}\rangle$, $G_{cc} = d\langle I_{Ca}\rangle/d[Ca^{2+}] = 10$ (in μA/cm^2 μM) is a negative-feedback gain parameter for the $[Ca^{2+}]$-dynamics (Ahmed et al., unpublished results), and

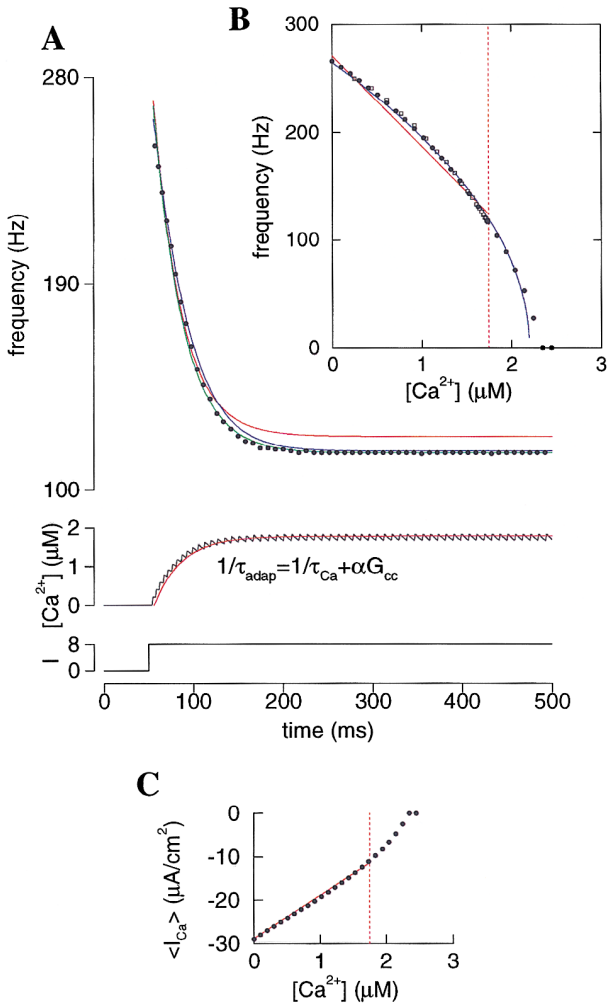

FIG. 2. Theoretical derivation of the spike-frequency adaptation time course. *A*: instantaneous firing rate [$f = 1/$interspike interval (ISI)] and $[Ca^{2+}]$ as function of time. *Red curves*: linear theory predictions. *Green curve*: empirical best fit. *Blue curve*: computed using a square-root fit for the *f*-vs.-$[Ca^{2+}]$ relation (see *B*). *B*: neuronal firing rate as function of $[Ca^{2+}]$. ●, data obtained when $[Ca^{2+}]$ was varied as a parameter. □, data from *A* with f plotted against $[Ca^{2+}]$ averaged over each individual ISI. Two data sets yield a same curve, demonstrating that the functional dependence of f on $[Ca^{2+}]$ can be obtained with $[Ca^{2+}]$ varied as a parameter. *Red curve*: linear regression fit; *blue curve*: square-root fit. *C*: average I_{Ca} as function of $[Ca^{2+}]$, fitted by a straight line *(red)*. In *B* and *C*, the dashed vertical lines indicate the plateau $[Ca^{2+}]$ level in *A*.

αG_{cc} (in 1/ms) is the rate at which the $[Ca^{2+}]$ influx is reduced by $[Ca^{2+}]$ itself.

In *step 2*, we turn to the $[Ca^{2+}]$ dynamics *Eq. 4*. Because it does not vary a lot within a sufficiently short ISI, I_{Ca} is substituted by $\langle I_{Ca}\rangle$, which is a function of $[Ca^{2+}]$. The resulting equation now only depends on $[Ca^{2+}]$

$$\frac{d[Ca^{2+}]}{dt} = (-\alpha \langle I_{Ca}\rangle_0) - [Ca^{2+}]/\tau_{adap} \quad (9)$$

with

$$\frac{1}{\tau_{adap}} = \alpha G_{cc} + \frac{1}{\tau_{Ca}} \quad (10)$$

Solving *Eq. 9*, we obtain

$$[Ca^{2+}](t) = [Ca^{2+}]_{ss}[1 - \exp(-t/\tau_{adap})] \quad (11)$$

with $[Ca^{2+}]_{ss} = -\alpha\langle I_{Ca}\rangle_0 \tau_{adap}$. Note that the adaptation time constant τ_{adap} (*Eq. 10*) is always smaller than τ_{Ca} due to the presence of the negative feedback term αG_{cc}. For instance, with $\alpha = 0.002$ and $G_{cc} = 10$, $\alpha G_{cc} = 0.02$ is larger than $1/\tau_{Ca} = 0.0125$, hence contributes more to τ_{adap}. We have $\tau_{adap} = 30.8$ ms, whereas $\tau_{Ca} = 80$ ms; and $[Ca^{2+}]_{ss} = 1.77$ μM.

Finally, in *step 3*, we insert the time course for $[Ca^{2+}]$ into the expression $f = f_0 - G_f[Ca^{2+}]$, which yields the adaptation process for the firing frequency as function of time

$$f(t) = f_{ss} + (f_0 - f_{ss})\exp(-t/\tau_{adap}) = 122 + 149\exp(-t/30.8) \quad (12)$$

with $f_{ss} = f_0 - G_f[Ca^{2+}]_{ss}$. The theoretically predicted time course for spike-frequency adaptation is shown in Fig. 2*A* (*red curve*), which compares well with the empirical fit (*green curve*). However, there is a small discrepancy between the numerical and predicted f_{ss}. This is mainly due to the fact that $f([Ca^{2+}])$ is not exactly linear. Indeed, f goes to zero at a critical value of $[Ca^{2+}] \simeq 2.2$ μM (when the I_{AHP} becomes too strong) via a homoclinic bifurcation of the saddle-node type. The mathematical theory of such a bifurcation predicts that, near the bifurcation, $f([Ca^{2+}])$ behaves as a square-root function of $[Ca^{2+}]$ (see Guckenheimer et al. 1997; Rinzel and Ermentrout 1987). We found that a square-root function fits well even the global $f([Ca^{2+}])$: $f([Ca^{2+}]) = 265\sqrt{1 - 0.455[Ca^{2+}]}$, *except* near the bifurcation threshold (Fig. 2*B*, *blue curve*). Using this nonlinear expression for $f([Ca^{2+}])$ and the same $[Ca^{2+}](t)$ as before, $f(t)$ can now be very accurately predicted (Fig. 2*A*, *blue curve*). In the following, we shall limit ourselves to the linear approximation.

Note that the percentage adaptation

$$F_{adap} = (f_0 - f_{ss})/f_0 = (-\alpha \langle I_{Ca}\rangle_0/f_0)G_f\tau_{adap} \quad (13)$$

which depends on the $[Ca^{2+}]$ dynamics and the I_{AHP} only through the factor $G_f\tau_{adap}$.

Calcium model of neuronal activity

We have described above how to reduce the biophysical membrane model of the neuron to a calcium-model, for a given applied current I

$$f(t) = [f_0(I) - G_f(I)[Ca^{2+}]]_+$$

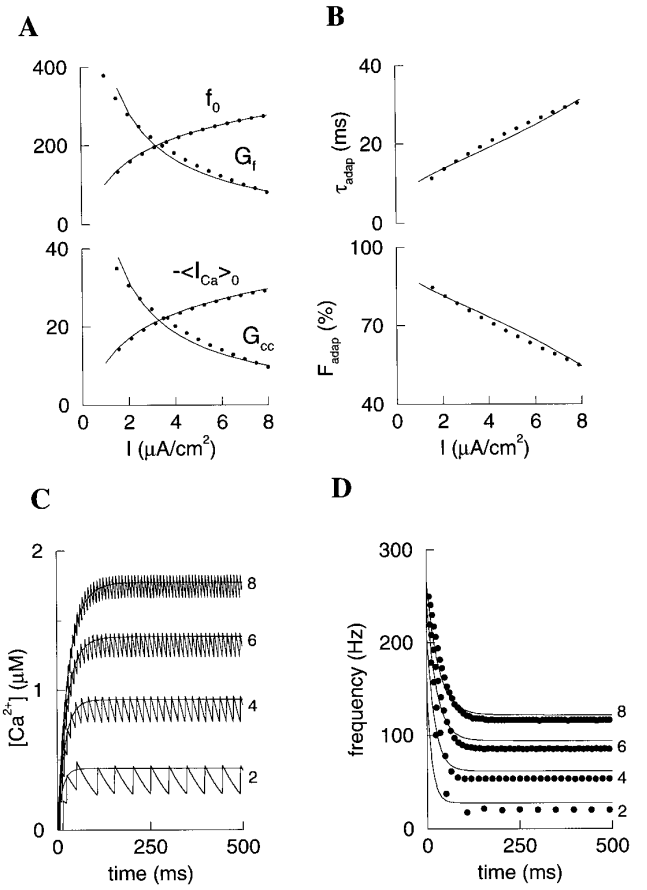

FIG. 3. Dependence on applied current intensity I. *A*: f_0, G_f, $\langle I_{Ca}\rangle_0$, and G_{cc} as functions of I. ——, empirical fitting functions of *Eq. 15*. *B*: adaptation time constant τ_{adap} increases, and the percentage adaptation F_{adap} decreases, with I. *C*: examples with 4 current intensities (indicated on the *right*), the smooth curves are theoretical predictions.

$$d[Ca^{2+}]/dt = -\alpha(\langle I_{Ca}\rangle_0(I) + G_{cc}(I)[Ca^{2+}]) - [Ca^{2+}]/\tau_{Ca} \quad (14)$$

where the firing rate is always positive by using the half-rectifying function $[x]_+ = x$ if $x \geq 0$, and 0 otherwise. The dependence on the current intensity I of the four quantities f_0, G_f, $\langle I_{Ca}\rangle_0$, and G_{cc} are shown in Fig. 3*A*. We observe that τ_{adap} is larger and F_{adap} is smaller with larger current intensities (see also Ahmed et al. unpublished results). This is because at higher I, spike width becomes slightly narrower, hence Ca^{2+} influx per spike is reduced. All four curves in Fig. 3*A* can be fitted reasonably well by logarithmic functions

$$f_0(I) = 9[\ln(I/0.3)]_+ \quad G_f(I) = 59 - 15[\ln(I/0.3)]_+$$

$$\langle I_{Ca}\rangle_0(I) = -84[\ln(I/0.3)]_+ \quad G_{cc}(I) = 551 - 143[\ln(I/0.3)]_+ \quad (15)$$

where $I_0 = 0.3$ is the estimated rheobase (The actual rheobase is somewhat larger, $I_0 \simeq 0.5$). Note that such a curve-fitting is purely empirical and is not based on theoretical grounds (see also Agin 1964; Koch et al. 1995).

Equations 14 and *15* completely describe the calcium model of neuronal activity. For this model to be useful, it should be able to predict the output firing rate $f(t)$, even when the input current $I(t)$ varies temporally in an arbitrary fashion. In Helmchen et al. (1996), the dendritic $[Ca^{2+}]$

signal was shown to encode firing frequency of a cortical layer V pyramidal neuron, when the input changed at the time scale of seconds. Intuitively, one expects that the calcium-model of neuronal discharges to be valid only when the temporal change of $I(t)$ is slower than both the individual ISIs and the $[Ca^{2+}]$ dynamics. Because of the adapting I_{AHP}, the effective $[Ca^{2+}]$ time constant is given by τ_{adap}, typically much shorter than τ_{Ca}. Hence, one can expect that the $[Ca^{2+}]$ code could remain effective even for input changes much more rapidly than in seconds. An example is shown in Fig. 4. Driven by a chaotic input current $I(t)$ (Fig. 4, *bottom*), the membrane potential fires spikes irregularly (Fig. 4, *top*). The instantaneous firing rate (the reciprocal of the ISI) and $[Ca^{2+}]$ as function of time are shown in Fig. 4, *middle* (in *blue*), superimposed with the predictions from the calcium-model (in *red*). This example suggests that the calcium model can indeed predict the instantaneous firing rate, even for relatively rapid time changes (within tens to hundreds of milliseconds) of the input current.

Dependence on the electrotonic coupling g_c

We next consider how the spike-frequency adaptation properties depend on the various biophysical parameters of the model. First, the spike-frequency adaptation is influenced strongly by the electrotonic coupling g_c, which controls the two-way current flow between the somatic and dendritic compartments. An example is illustrated in Fig. 5*A*, with two different values of g_c and a same current pulse to the soma. With a larger g_c, there is greater current loss to the dendrite, hence the initial firing frequency is lower (Fig. 5*A*, *left*). On the other hand, the dendritic membrane potential repolarizes more rapidly after the somatic spike, the dendritic spike width is narrower, and the $[Ca^{2+}]$ influx per spike is reduced (Fig. 5*A*, *right*). This leads to a slower $[Ca^{2+}]$ accumulation, larger τ_{adap}, and smaller percentage adaptation F_{adap} (Fig. 5*B*). As in the case of varying the applied current I (Fig. 3*B*), the two quantities τ_{adap} and F_{adap} change in an antagonistic manner (faster adaptation time course is correlated with a greater degree of adaptation).

On the other hand, *burst firing* of spikes can be observed when the electrotonic coupling g_c between the two compartments is sufficiently small, and the dendritic membrane area is significantly larger than the somatic one so that the coupling is asymmetric and the soma-to-dendrite influence is weak (Mainen and Sejnowski 1996; Pinsky and Rinzel 1994; Rhodes and Gray 1994; Traub 1982; Traub et al. 1994). Similar to the *intrinsically bursting* pyramidal cells in layer V neocortex (Kim and Connors 1993; Mason and Larkman 1990; McCormick et al. 1985; Nishimura et al. 1996), with moderate current intensity the model neuron fires doubles of spikes repetitively at low frequencies ($\sim$4 Hz); and (more typically) current injection of higher intensities elicits an initial burst of spikes followed by a train of single spikes (Fig. 5*C*). This firing pattern can be viewed as an extremely strong form of spike-frequency adaptation, produced by the same set of ion channels as the adaptation phenomenon (if these ion channels are located at dendritic sites sufficiently isolated from the soma).

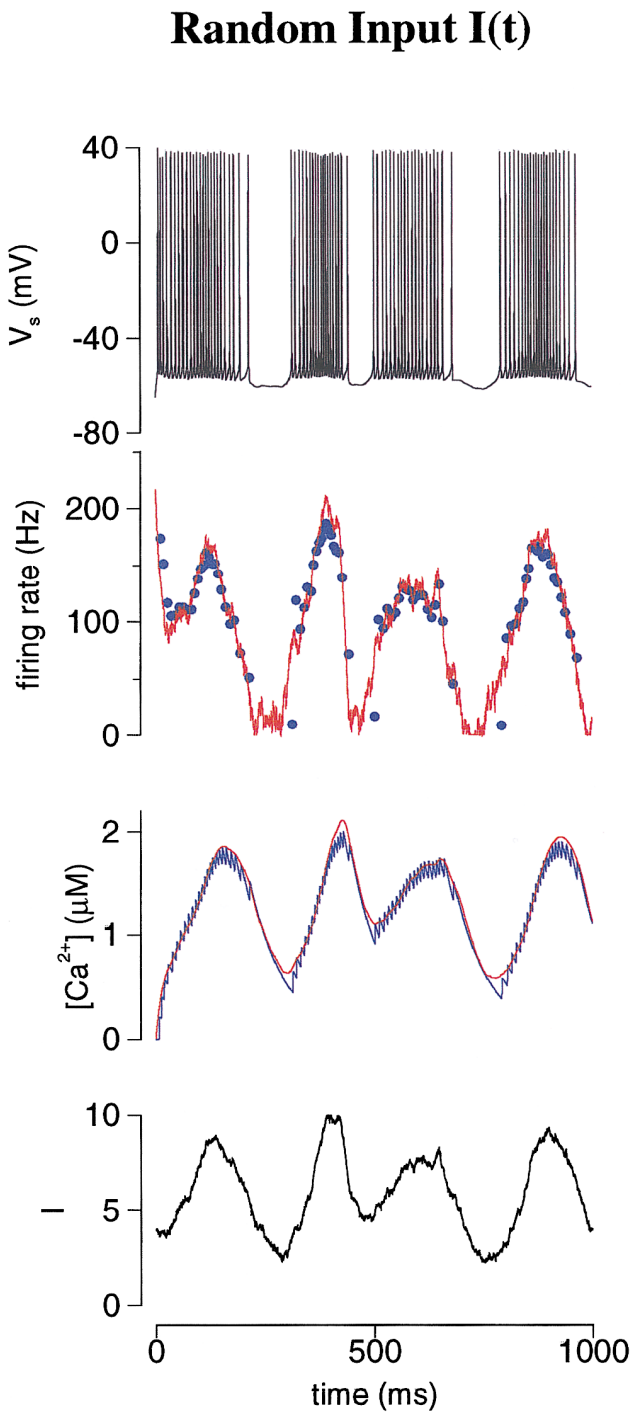

FIG. 4. Calcium coding of neuronal electrical activity. In response to a temporally varying input $I(t)$ (*bottom*), the cell's firing (*blue dots, middle top*) and $[Ca^{2+}]$ time course (*blue curve, middle bottom*) are well predicted by the reduced calcium model *Eqs. 14* and *15 (red curves)*.

Relations between τ_{adap} and F_{adap}

In addition to the neuronal electrotonic structure, spike-frequency adaptation depends also on the channel conductances g_{Ca} and g_{AHP}, as well as the $[Ca^{2+}]$ kinetic parameters α and τ_{Ca}. These dependences were explored within the framework of our calcium-model. First, the initial firing rate

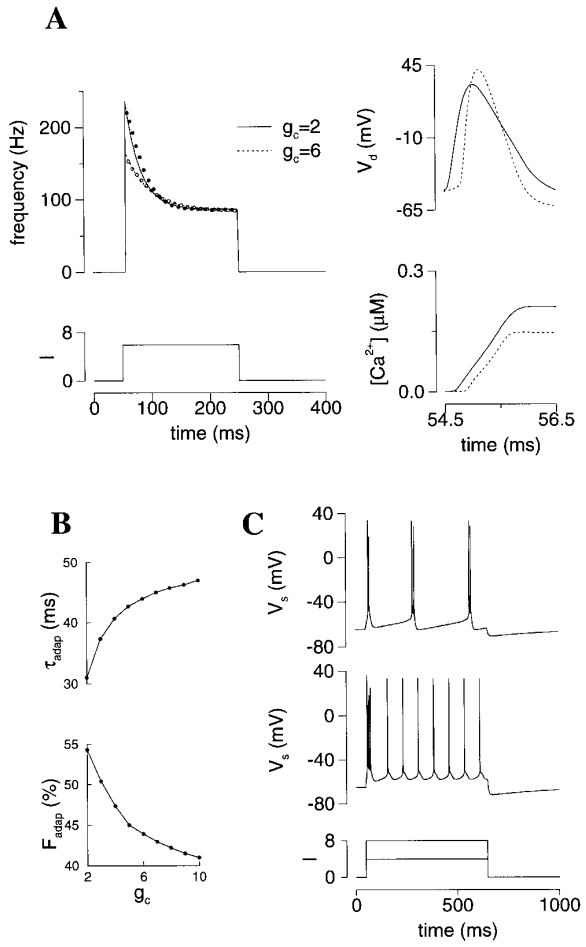

FIG. 5. Dependence on the electrotonic coupling g_c between the 2 compartments. *A*: with an increased g_c, the initial firing frequency is lower but the steady-state frequency remains the same (*left*). Reduced percentage adaptation is due to a narrower dendritic spike (because V_d repolarizes more rapidly at larger g_c), hence a smaller $[Ca^{2+}]$ influx per spike (*right*). *B*: τ_{adap} increases, and F_{adap} decreases, with g_c. *C*: burst firing patterns with modified electrotonic properties ($g_c = 1.4$, $P = 0.3$) and $g_{Ca} = 0.5$, $g_{AHP} = 18$.

f_0 should not depend on any of these parameters. Second, because $\langle I_{Ca}\rangle = \langle I_{Ca}\rangle_0 + G_{cc}[Ca^{2+}]$, $\langle I_{Ca}\rangle_0$ and G_{cc} should be proportional to g_{Ca}. Third, both gain parameters G_f and G_{cc} must be proportional to g_{AHP}. In summary, we can write

$$G_f = \bar{G}_f g_{AHP}, \quad \langle I_{Ca}\rangle_0 = \langle \bar{I}_{Ca}\rangle_0 g_{Ca}, \quad G_{cc} = \bar{G}_{cc} g_{Ca} g_{AHP} \qquad (16)$$

Inserting these scaling relations into *Eqs. 10* and *13* we have

$$1/\tau_{adap} = (\alpha g_{Ca} g_{AHP})\bar{G}_{cc} + 1/\tau_{Ca}$$

$$F_{adap} = (\alpha g_{Ca} g_{AHP})(-\bar{G}_f \langle \bar{I}_{Ca}\rangle_0 / f_0)\tau_{adap} \qquad (17)$$

From *Eq. 17* we can conclude that τ_{adap} and F_{adap} depend only on τ_{Ca} (a neuron's $[Ca^{2+}]$ extrusion and buffering properties) and on the combination $\alpha g_{Ca} g_{AHP}$ (the product of the spike-evoked $[Ca^{2+}]$-influx size αg_{Ca} and the adaptation conductance g_{AHP}). Given fixed $\alpha g_{Ca} g_{AHP}$, as τ_{Ca} is increased (Fig. 6*A*), the adaptation is slower (τ_{adap} is larger), but the plateau $[Ca^{2+}]$ level is higher (cf. *Eqs. 4* and *11*), hence F_{adap} is larger. A plot of F_{adap} versus τ_{adap} is linear with a positive slope (Fig. 6*B*). This is evident in *Eq. 17*, where f_0, $\bar{G}_f$, and $\langle I_{Ca}\rangle_0$ (computed with $[Ca^{2+}]$ as a static parameter) are all independent of τ_{Ca}, hence F_{adap} is simply proportional to τ_{adap}. The slope of the linear curve, however, depends on the input current intensity I.

By contrast, if τ_{Ca} is held constant and $\alpha g_{Ca} g_{AHP}$ is increased (Fig. 6*C*), adaptation is faster (τ_{adap} is smaller) and the percentage adaptation F_{adap} is larger. The plot of F_{adap} versus τ_{adap} shows a linear relation with a negative slope (Fig. 6*D*). In Fig. 6*D*, we also plotted the F_{adap} versus τ_{adap} simulation data, obtained when the input current intensity I is varied (Fig. 3*B*) and when the electrotonic coupling g_c is varied (Fig. 5*B*). Quite surprisingly, in all cases, the F_{adap}-τ_{adap} curve is linear with approximately the same slope $\simeq 1/65$, which is close to, but differs from, the reciprocal of the $[Ca^{2+}]$ decay time constant $1/\tau_{Ca} = 1/80$.

To gain some insights about this general relation between F_{adap} and τ_{adap}, let us suppose that the ratio between the initial value and the gain parameter is roughly the same for f and $\langle I_{Ca}\rangle$, i.e., $f_0/G_f \simeq (-\langle I_{Ca}\rangle_0)/G_{cc}$. With this assumption, we then can write $-\langle I_{Ca}\rangle_0 G_f/f_0 \simeq G_{cc}$. Inserting this relation into *Eq. 13*, we have

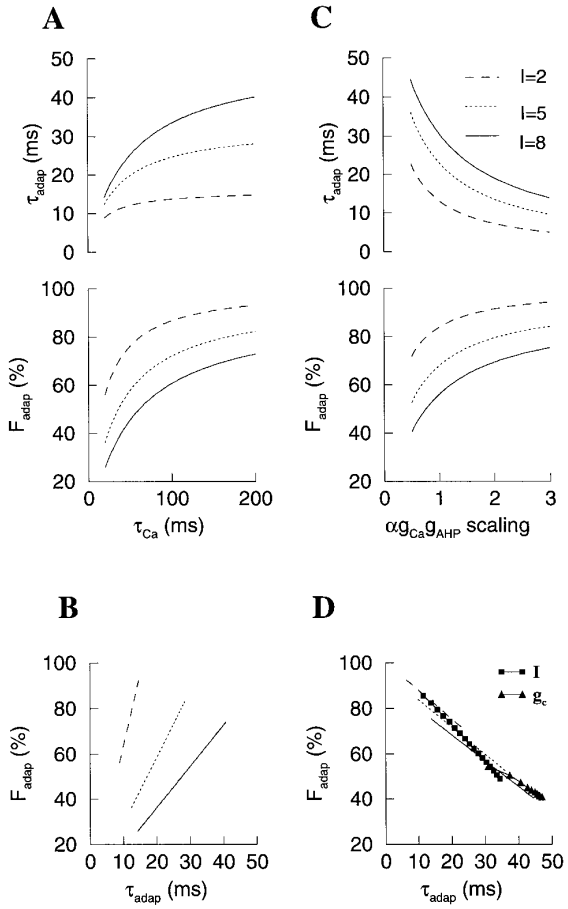

FIG. 6. Dependence of τ_{adap} and F_{adap} on τ_{Ca} (*A* and *B*) and the combination $\alpha g_{Ca} g_{AHP}$ (*C* and *D*) (cf. *Eq. 17*). Three curves in each panel correspond to different applied current intensities. *B*: F_{adap} vs. τ_{adap} from data in *A* is linear with a positive slope (which depends on *I*). *D*: F_{adap} vs. τ_{adap} from data in *C*: is linear with a negative slope $\simeq -1/\tau_{Ca}$. This is also true for data obtained with *I* (Fig. 3*B*) or g_c (Fig. 5*B*) being varied as parameter.

$$F_{adap} \simeq \alpha G_{cc} \tau_{adap} \quad (18)$$

or because $\alpha G_{cc} = 1/\tau_{adap} - 1/\tau_{Ca}$ (*Eq. 10*), we have

$$F_{adap} \simeq 1 - \tau_{adap}/\tau_{Ca} \quad (19)$$

which is the desired relation between F_{adap} and τ_{adap}. This theoretical prediction is directly testable by experimental measurements from cortical pyramidal neurons.

Two calcium modes

We have developed our calcium model of neuronal activity *Eqs. 14* and *15* with the ion currents I_{Ca} and I_{AHP} localized at the dendrite. In real cortical pyramidal neurons, of course, these channels are distributed widely on the dendritic trees as well as the soma (Jaffe et al. 1994; Johnston et al. 1996; Yuste et al. 1994). It is of interest to investigate whether our approach can be generalized to such cases where the $[Ca^{2+}]$ signaling and $[Ca^{2+}]$-dependent spike-frequency adaptation are distributed across multiple compartments. For our two-compartment model, suppose that the distributions of g_{Ca} and g_{AHP} are uniform at the soma and dendrite, $g_{Ca} = 1$ and $g_{AHP} = 5$ (in mS/cm^2) for both compartments. We then have two equations like *Eq. 4* for somatic and dendritic $[Ca^{2+}]$, respectively

$$\frac{d[Ca^{2+}]_s}{dt} = -\alpha_s I_{Ca,s} - [Ca^{2+}]_s/\tau_{Ca,s}$$

$$\frac{d[Ca^{2+}]_d}{dt} = -\alpha_d I_{Ca,d} - [Ca^{2+}]_d/\tau_{Ca,d} \quad (20)$$

Because the parameter α is proportional to the surface:volume ratio, it should be much smaller for the soma than for the dendrite. Similarly, τ_{Ca} is expected to be longer at the soma than at the dendrite. For instance, the spike-evoked $[Ca^{2+}]$ transient peak amplitude and decay rate ($1/\tau_{Ca}$) can be three times as large in some dendritic sites as in the soma (Schiller et al. 1995). With the simple two-compartment model, let us assume that for the dendritic compartment, $\alpha_d = 0.002$ and $\tau_{Ca,d} = 80$ ms, whereas for the somatic compartment we multiple the right-hand side of *Eq. 4* by a factor of $\frac{1}{3}$, so that $\alpha_s = 0.000667$ and $\tau_{Ca,s} = 240$ ms. As shown in Fig. 7, with two calcium modes, $[Ca^{2+}]_s(t)$, $[Ca^{2+}]_d(t)$, and $f(t)$ can be empirically well fitted by a sum of two exponentials, with the first rapid phase followed by a second much slower phase (Fig. 7, *red curves*)

$$[Ca^{2+}]_s(t) = 0.74 - 0.3\exp(-t/\tau_{adap,1}) - 0.44\exp(-t/\tau_{adap,2})$$

$$[Ca^{2+}]_d(t) = 1.13 - 1.63\exp(-t/\tau_{adap,1}) + 0.5\exp(-t/\tau_{adap,2})$$

$$f(t) = 73 + 225\exp(-t/\tau_{adap,1}) + 16\exp(-t/\tau_{adap,2}) \quad (21)$$

where $\tau_{adap,1} = 29.4$ ms and $\tau_{adap,2} = 191$ ms. None that the faster $[Ca^{2+}]$ mode (which is primarily of the dendritic origin) dominates the spike-frequency adaptation, while the slower mode is only $16/225 = 7\%$ of the faster mode. Moreover, the time course of $[Ca^{2+}]_d$ can be nonmonotonic (Fig. 7). In the first rapid phase of adaptation, $[Ca^{2+}]_s$ is small, both $[Ca^{2+}]_d$ and the firing rate converge to their plateau levels as if the somatic I_{AHP} did not exist. But as $[Ca^{2+}]_s$ (hence the somatic I_{AHP}) slowly accumulates, the firing rate further decreases in the second phase of adaptation, which leads to a *decay* of $[Ca^{2+}]_d$ to its actual final plateau, which is *smaller* than would be expected without a somatic I_{AHP}. Hence, the nonmonotonic behavior of $[Ca^{2+}]_d(t)$.

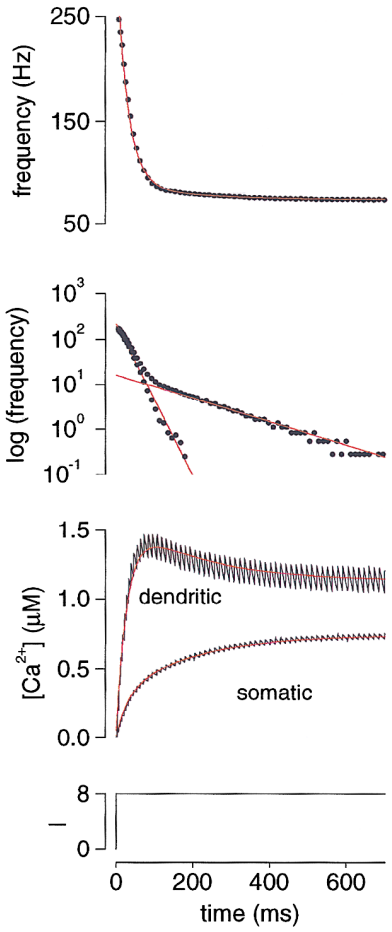

FIG. 7. Two Ca^{2+} modes. With g_{Ca} and g_{AHP} on both the somatic and dendritic compartments, the time course of spike-frequency adaptation is a sum of 2 exponentials, with $\tau_{adap,1} = 29.4$ ms and $\tau_{adap,2} = 191$ ms. Faster component (largely due to the dendritic g_{AHP}) dominates (*top*). Dendritic $[Ca^{2+}](t)$ is not monotonic and displays a maximum at around $t_{max} = 106$ ms. *Red curves*: empirical fits.

The theoretical analysis for the adaptation time course can be generalized in this case, but only approximately. As is detailed in APPENDIX C, our liner approach yields good estimates for the two adaptation time constants $\tau_{adap,1}$ and $\tau_{adap,2}$. However, the steady state plateaus and the actual time courses cannot be predicted accurately unless nonlinear interactions between the two $[Ca^{2+}]$ modes are taken into account.

Adaptation to stochastic Poisson input

So far, spike-frequency adaptation of cortical pyramidal neurons has been investigated with current pulse stimulation. However, in in vivo conditions, pyramidal cells are driven by synaptic inputs that are stochastic and vary unceasingly in time. As a first step toward addressing the question of spike-frequency adaptation to natural stimuli, we stimulated the response of our model neuron to random synaptic inputs

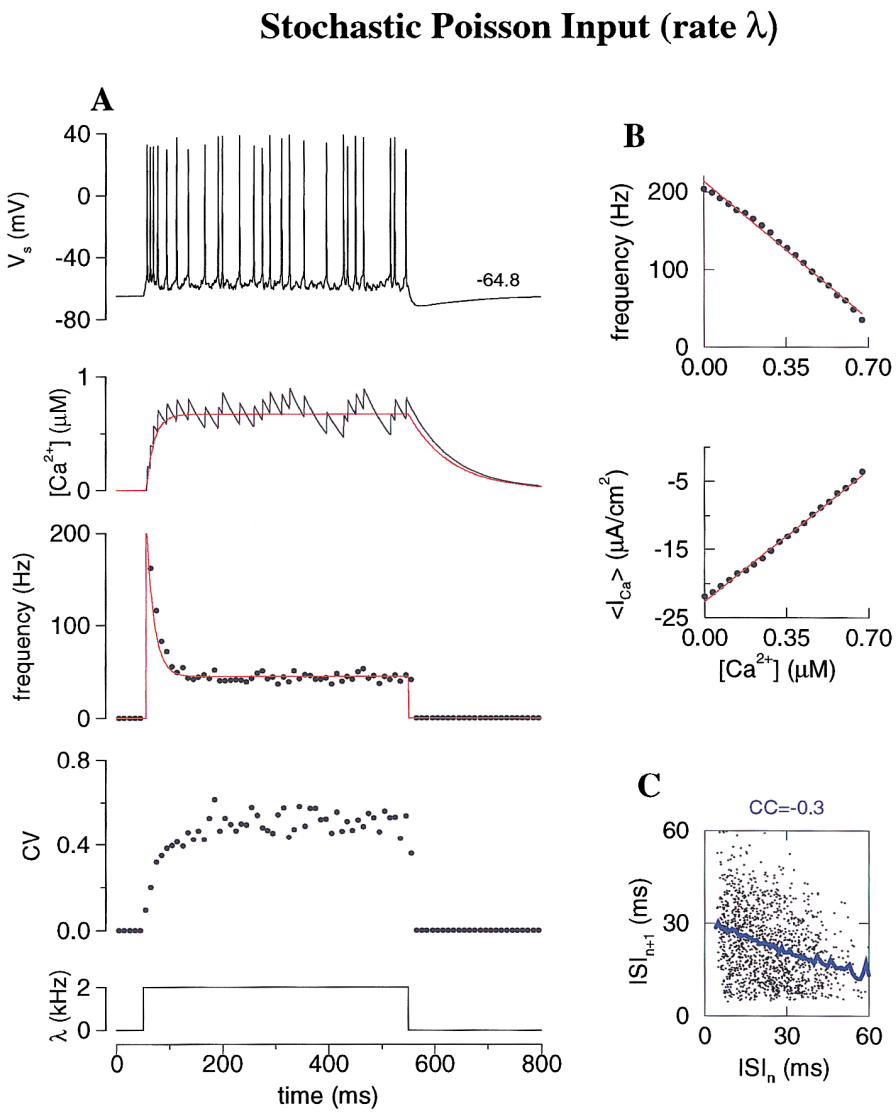

FIG. 8. Adaptation to a Poisson synaptic input. *A*: an example of the membrane potential and $[Ca^{2+}]$ time course (*top* and *middle top*). Cell initially fires rapidly that appears as a burst of spikes, followed by a firing pattern that is uneven in time. Instantaneous firing rate (averaged over 100 trials) has a single exponential time course (*middle bottom*). ISI variability increases with decreasing firing rate (*bottom*). *Red curves*: theoretical predictions. *B*: linear dependence of f and $\langle I_{Ca}\rangle$ on $[Ca^{2+}]$. *C*: ISI return map (t_{n+1} vs. t_n). *Blue curve*: conditional average of t_{n+1} for each fixed t_n, which is approximately linear with a negative slope $\kappa = -0.3$. (Dendritic $g_{AHP} = 8$ mS/cm^2.)

generated by a Poisson process with rate λ. As illustrated in Fig. 8*A*, when the Poisson input is turned on, the cell initially fires rapidly (at 180 Hz), then the firing rate is reduced in parallel with the accumulation of $[Ca^{2+}]$. The instantaneous firing frequency calculated by averaging over trials shows a time course similar to that with a constant current pulse. This time course can be predicted using the same analysis as before, except that now we use *trial-averaged* firing rate f and calcium current I_{Ca}. As shown in Fig. 8*B*, both f and $\langle I_{Ca}\rangle$ are approximately linear with $[Ca^{2+}]$ when the latter is considered as a parameter

$$f = f_0 - G_f[Ca^{2+}]; \quad \langle I_{Ca}\rangle = \langle I_{Ca}\rangle_0 + G_{cc}[Ca^{2+}] \qquad (22)$$

where $f_0 = 213$ Hz, $G_f = 252$ Hz/μM, $\langle I_{Ca}\rangle_0 = -22.6$ μA/cm^2, and $G_{cc} = 27.5$ μA/cm^2 μM. Solving *Eq. 4* with I_{Ca} substituted by $\langle I_{Ca}\rangle$, we obtain

$$[Ca^{2+}](t) = [Ca^{2+}]_{ss}(1 - \exp(-t/\tau_{adap}))$$
$$f(t) = f_{ss} + (f_0 - f_{ss})\exp(-t/\tau_{adap}) \qquad (23)$$

where $\tau_{adap} = 14.8$ ms, $[Ca^{2+}]_{ss} = 0.67$ μM, $f_{ss} = 44.2$ and $f_0 = 213$ (in Hz). (Note, again, τ_{adap} is much shorter than $\tau_{Ca} = 80$ ms.) These curves fit accurately with the simulation data (red curves in Fig. 8*A*).

Driven by random EPSPs, the neuronal firing activity displays fluctuations. We calculated the coefficient of variation of the ISIs (cf. METHODS). The CV displays a time course that mirrors the mean instantaneous firing rate (Fig. 8*A*): its initial value is low but not zero (~0.1), increases as the firing rate decreases, and plateaus at a value close to 0.5. The ISI variability is expected to be larger with lower firing frequencies when the cell acts more like a coincidence detector than a temporal integrator of excitatory inputs (Perkel et al. 1967; Softky and Koch 1993; Stern 1965).

Because the firing is now random, the membrane potential shows two noteworthy features. First the initial response appears as a burst, even though the neuron shows typical adaptation time course and no burst with a current pulse (Fig. 1). Second, in the steady state after the transient burst, fast doublets can be observed typically after a relatively long silent time. This phenomenon can be understood in terms of

temporal correlations caused by the spike-adapting current I_{AHP}. Statistically, if by chance the cell happens to fire rapidly in a short time window, significant $[Ca^{2+}]$ influx will be produced, the enhanced I_{AHP} will hyperpolarize the cell, and the firing rate subsequently will be reduced. Conversely, during a time period of relative low firing, I_{AHP} decreases as a result of the $[Ca^{2+}]$ decay, and the probability of firing increases. In short, the adaptation generates *negative* statistical temporal correlations between ISIs. This is shown in Fig. 8*C* by the ISI return map (computed in the steady state) where the $(n + 1)$th ISI is plotted against the nth ISI. Given ISI_n, the average ISI_{n+1} is calculated (*blue curve*) and yields a linear relation with a slope $\kappa = -0.3$. This slope is the same as the coefficient of correlation between successive ISIs (the CC, see METHODS). It is about a third of the maximum negative correlation ($\kappa = -1$) possible.

The steady-state input-output relation, i.e., the mean firing rate f versus the Poisson input rate λ, is linear (Fig. 9*A*, *red curve*). We also computed the ISI CV and CC as function of λ; they are plotted against the mean output frequency f (Fig. 9, *B* and *C*). One observes that the CV changes slightly with f, ranging 0.3–0.5 (Fig. 9*B*, *red curve*). The CC shows a much stronger frequency dependence with a large negative peak at $f \simeq 20$ Hz (Fig. 9*C*, *red curve*). This strong frequency dependence can be explained in terms of two time constants: $\tau_{Ca} = 80$ ms and $\tau_{adap} \simeq 15$ ms (for the sake of argument, we assume that τ_{adap} remains about the same as λ is varied). The negative ISI correlation is produced by the spike-adapting current I_{AHP}, and the effect is large only in a neuronal firing rate range such that the mean ISI $(1/f)$ is between τ_{adap} and τ_{Ca}. This is because when the firing rate f is very low ($f < 1/\tau_{Ca} \sim 10$ Hz), $[Ca^{2+}]$ decays back to baseline between spikes so that I_{AHP} cannot accumulate and $\kappa \simeq 0$. On the other hand, at very high firing rates ($f > 1/\tau_{adap} \sim 70$ Hz), no significant adaptation dynamics takes place during two *consecutive* ISIs, and their correlation should again be small.

This result demonstrates that, when the input is stochastic, the $[Ca^{2+}]$-dependent current I_{AHP} strongly sculptures the firing patterns by producing negative correlations between ISIs in a frequency-dependent manner, *even in the stationary state* where the trial-averaged firing rate is constant.

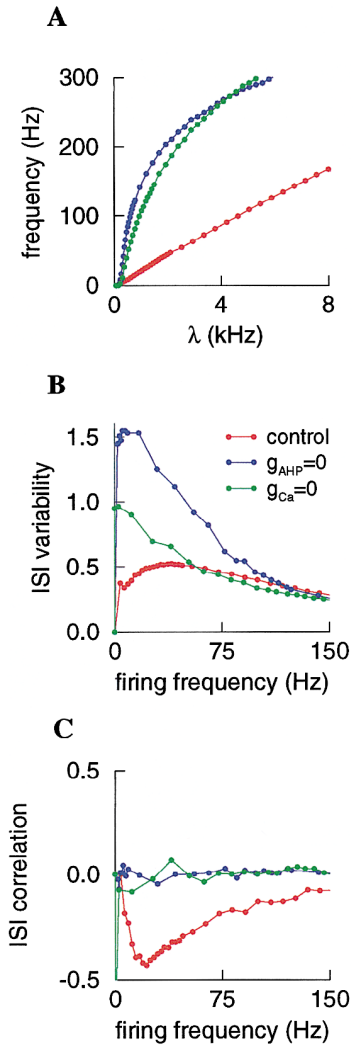

FIG. 9. Dependence on the Poisson input rate λ. *A*: average steady-state firing rate f as function of λ. ISI variability (CV) *(B)* and ISI correlation (CC) *(C)* are plotted as function of f. *Red*: control (with dendritic $g_{Ca} = 1$ and $g_{AHP} = 8$ mS/cm^2), *blue*: $g_{AHP} = 0$, *green*: $g_{Ca} = 0$. Note that when $g_{AHP} = 0$ but g_{Ca} is present, the CV is larger than 1 at low firing frequencies *(B)*. On the other hand, the CC is virtually 0, hence the ISIs are essentially uncorrelated in time when $g_{AHP} = 0$ *(C)*. In control condition, CC depends strongly on firing frequency and displays a negative peak at $\simeq 20$ Hz.

Stochastic burst firing

We confirmed that the ISI correlation (CC) is essentially zero when the spike-frequency adaptation is absent by blocking either g_{AHP} or g_{Ca} (Fig. 9*C*, *blue* and *green curves*). Interestingly, with $g_{AHP} = 0$, the ISI variability (CV) is >1 at low frequencies, whereas it is always <1 if $g_{Ca} = 0$ (Fig. 9*B*). Note that the behavior with $g_{AHP} = 0$ should be the same as the initial unadapted firing state when g_{AHP} is not blocked (but $I_{AHP} = 0$). Therefore, the f-λ curves with or without g_{AHP} blockade in Fig. 9*A* can be considered as the initial and the plateau input-output relations, respectively, under control conditions.

The firing is highly irregular (with CV > 1) when the g_{AHP} is blocked because of a hysteresis phenomenon that is produced by a dendritic calcium plateau potential (cf. Marder et al. 1996). Indeed, when the neuron model is excited by a constant input current (within an appropriate range), there is a bistability where both the resting state and a state of repetitive spiking are possible (data not shown). Because Poisson synaptic inputs are not constant in time, the model neuron is driven to switch randomly between the two states (Fig. 10*A*). There is no significant ISI correlation in the absence of I_{AHP} (Fig. 10*B*). The switching is not periodic but stochastic, and the ISI distribution is not bimodal (Fig. 10*C*). The large CV is related to the presence of a long tail in the ISI distribution, with large ISIs corresponding to the time epochs when the cells is in the silent state (Fig. 10*C*). Note that hysteresis between two states has been suggested previously to be a cause of large ISI variability, although in these cases the ISI distribution is bimodal (Stern et al. 1997; Wilbur and Rinzel 1983). Such

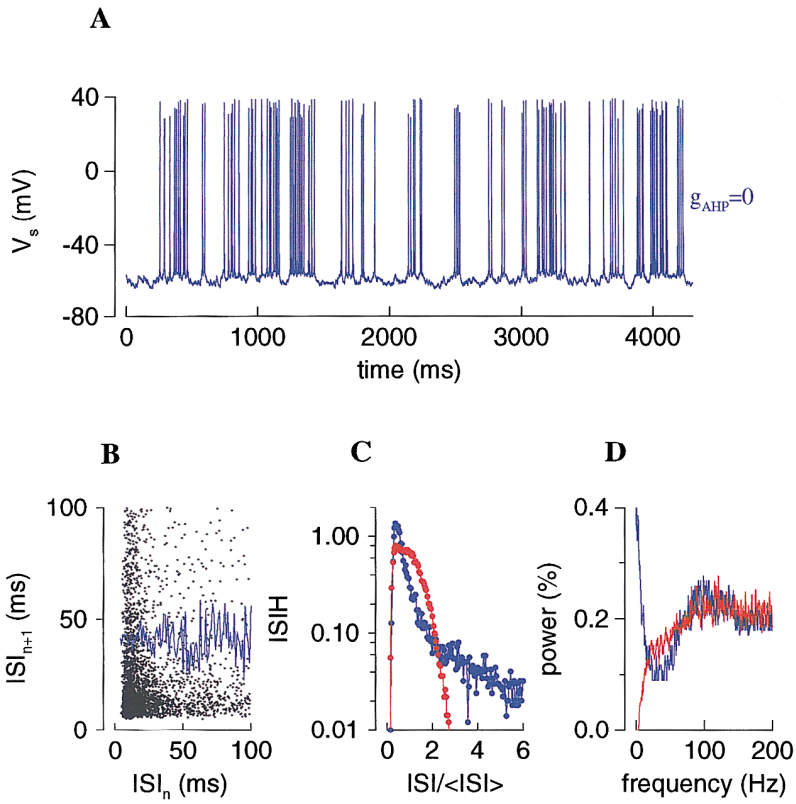

FIG. 10. *A*: an example with $g_{AHP} = 0$ and $\lambda = 0.3$ kHz, which shows high ISI variability (CV > 1). Membrane potential randomly switches in time between a resting (inactive) phase and a firing (active) phase. *B*: consecutive ISIs are not correlated in time. *C*: ISI distribution shows a long tail that spans several mean ISI *(blue curve)*, in contrast with the case of Fig. 8 with adaptation *(red curve)*. ISI distributions are plotted against ISI/⟨ISI⟩. *D*: power spectrum of the spike train has a large amplitude at low frequencies *(blue curve)*, whereas the adaptation current I_{AHP} filters out response power at low-frequencies *(red curve)*.

dynamics with many long time scales also is reflected in the power spectrum of the spike train, which displays large amplitudes at low frequencies (Fig. 10*D, blue curve*). By contrast, in an adapting state with $g_{AHP} \neq 0$, powers at lower frequencies are strongly suppressed (Fig. 10*D, red curve*). Such high-pass filtering behavior is a common and important signature of temporally adapting dynamics.

Although random switching between two states gives rise to an apparently bursty pattern of neuronal firing (Fig. 10), we emphasize that it is very different from an intrinsically bursting behavior that does not require random switching by fluctuating inputs. We simulated the bursting state of Fig. 5*C* with Poisson inputs (Fig. 11). In this case, the membrane potential displayed a temporal mixture of single spikes and bursts of spikes (Fig. 11*A*). Unlike the bistable dynamics, bursting state showed a large negative correlation between ISIs due to the g_{AHP} (Fig. 11*B*). Furthermore, the ISI distribution can be bimodal: a broad peak at typical ISI values between single spikes, whereas a second sharp peak at ISI $\simeq$ 3–5 ms corresponds to the short ISIs within a burst (Fig. 11*C*). The bimodality is most evident at low mean firing rates when the two maxima are well separated (Fig. 11*C, blue* and *red curves*). The bimodality also is reflected by the presence of a distinct peak in the power spectrum of spike trains (Fig. 11*D*). At higher mean firing rates, the broad peak moves closer to, and eventually overlaps with, the sharp peak of the ISI distribution (Fig. 11*C, black curve*), and the hump in the power spectrum disappears (Fig. 11*D*).

To summarize, stochastic switching between a resting state and a firing state is characterized by a long tail in the ISI distribution and a high power at low frequencies. By contrast, an intrinsically bursting neuron is characterized by a random temporal mixture of bursts and single spikes, a strong negative ISI correlation, a bimodal ISI distribution and a peak in the power spectrum that depends on the level of the excitatory drive.

Forward masking

We investigated possible computational implications of the spike-frequency adaptation, in particular a ''forward masking'' effect suggested by the experiments of Sobel and Tank (1994) on the cricket Omega auditory neurons. Namely, when two or several inputs are presented sequentially in time, neuronal response to the first input would activate an I_{AHP} with a delay, thereby inhibiting responses to subsequent inputs. To see if such an effect also occurred in our pyramidal neuron model, we first presented to the cell a ''masking'' input pulse, then a test input pulse after a time interval of τ ms (Fig. 12). Indeed, the response to the test input was reduced dramatically by the masking input (Fig. 12, *A* and *B*). The peak response to the test input was decreased in proportion with the amplitude of the masking input, i.e., there was a linear relationship between the two with a negative slope (Fig. 12*C*). The masking effect was produced by the residual $[Ca^{2+}]$, which was accumulated by the neuronal firing during the masking input and which did not have enough time to return to its baseline between the two pulses as long as τ was not too large. Therefore, a significant amount of residual I_{AHP} inhibited the neuronal

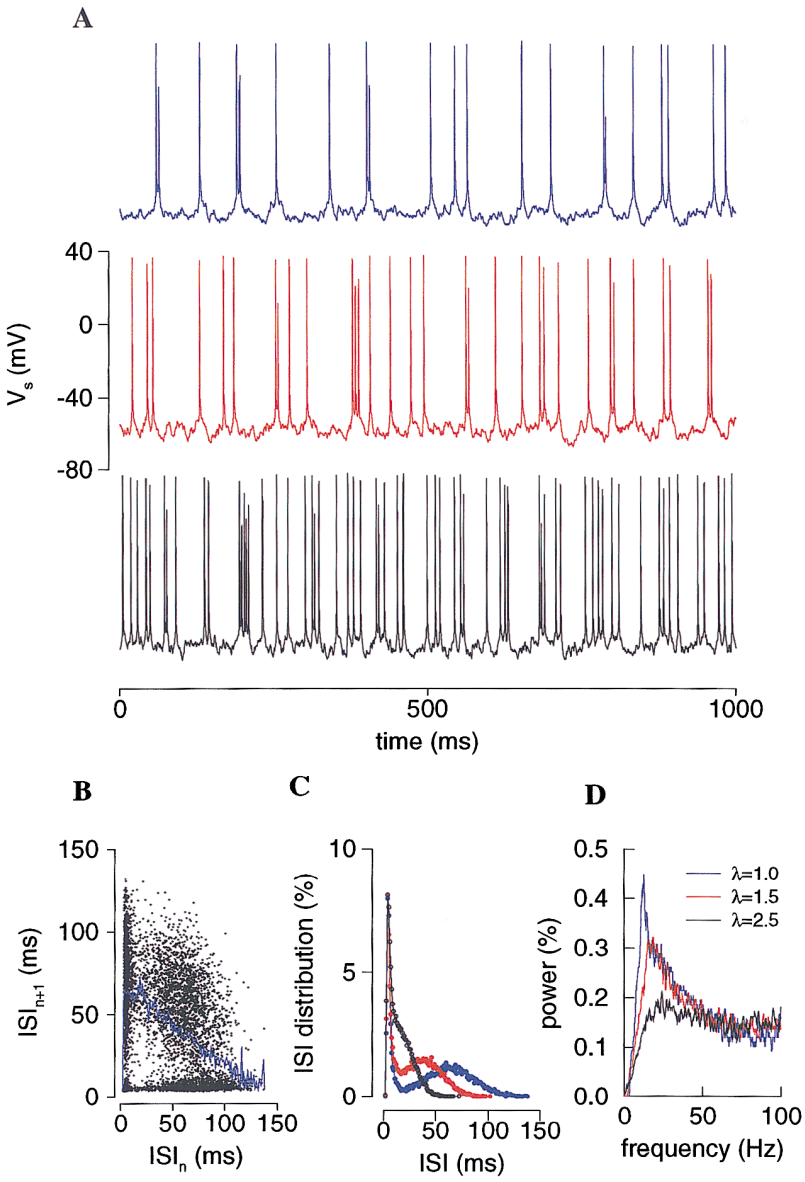

FIG. 11. Burst firing pattern by Poisson input. *A*: in the bursting regime (with the same parameters as in Fig. 5*C*), the cell's response to random synaptic inputs typically show a temporal mixture of single spikes and bursts of spikes. From *top* to *bottom*: $\lambda = 1.0$, 1.5, and 2.5 kHz. *B*: ISI return map for *top panel* in *A*, showing a strong negative correlation between the consecutive ISIs (*blue curve*: conditional average of t_{n+1} for given t_n). *C*: ISI distributions for the 3 examples in *A*. There is a bimodality at low rates (*blue* and *red*). An increased firing frequency shifts the second peak to the left, so that the 2 peaks overlap with each other (*black*). *D*: bimodality of the ISI distribution indicates a statistical repetition of the firing events in time, which is reflected in the power spectra of the spike train by the presence of a significant peak (*blue* and *red*). Peak disappears when the ISI distribution is no longer bimodal (*black*).

firing at the onset of the test pulse. Interestingly, there is often a time lag between the test input onset and neuronal response, which allows $[Ca^{2+}]$ to decay further and leads to a gradually increasing time course of the neuronal response (Fig. 12*B*). The requirement for the relative timing of the two inputs can be quantified by plotting the ratio of the two peak responses f_2/f_1 versus τ. The recovery follows a decay time course like $\sim\exp(-\tau/\tau_{Ca})$ (Fig. 12*D*). This is expected because it should be the same as the decay time course of $[Ca^{2+}]$ during the time τ, which, in the absence of spike-triggered influx, satisfies $d[Ca^{2+}]/dt = -[Ca^{2+}]/\tau_{Ca}$.

When two or several inputs of different amplitudes are presented to the neuron model, one expects that the forward masking mechanism can produce a ''selective attention'' effect where responses to all inputs but the strongest one are suppressed (Pollack 1988). This is illustrated with two periodic trains of pulses with different amplitudes (Fig. 13*A*). As is shown in Fig. 13*B*, the input-output relation for the *stimulus 2* is approximately linear; the presence of *stimulus 1* shifts this response curve to higher input rates, but does not significantly change its slope (cf. Fig. 1C in Sobel and Tank 1994). Note that because the inputs were repetitive and $[Ca^{2+}]$ accumulated between pulses, firing responses to both stimuli were affected by the adaptation dynamics: each was smaller than what it would have been in the absence of the other input. However, the effect was differential and the reduction was much smaller to the response to stronger input than that to the weaker one. This was shown by plotting the ratio of responses f_2/f_1 versus that of inputs λ_2/λ_1, which yields a very nonlinear curve (Fig. 13*C*). For example, if the *stimulus 1* input rate is twice that of *stimulus 2*, the response to *stimulus 1* was 25 times that of *response 2* (Fig. 13*C*). Therefore, in the presence of two or more inputs, the $[Ca^{2+}]$-dependent adaptation process can selectively suppress the neuronal responses to weaker inputs so that the response to the strongest input

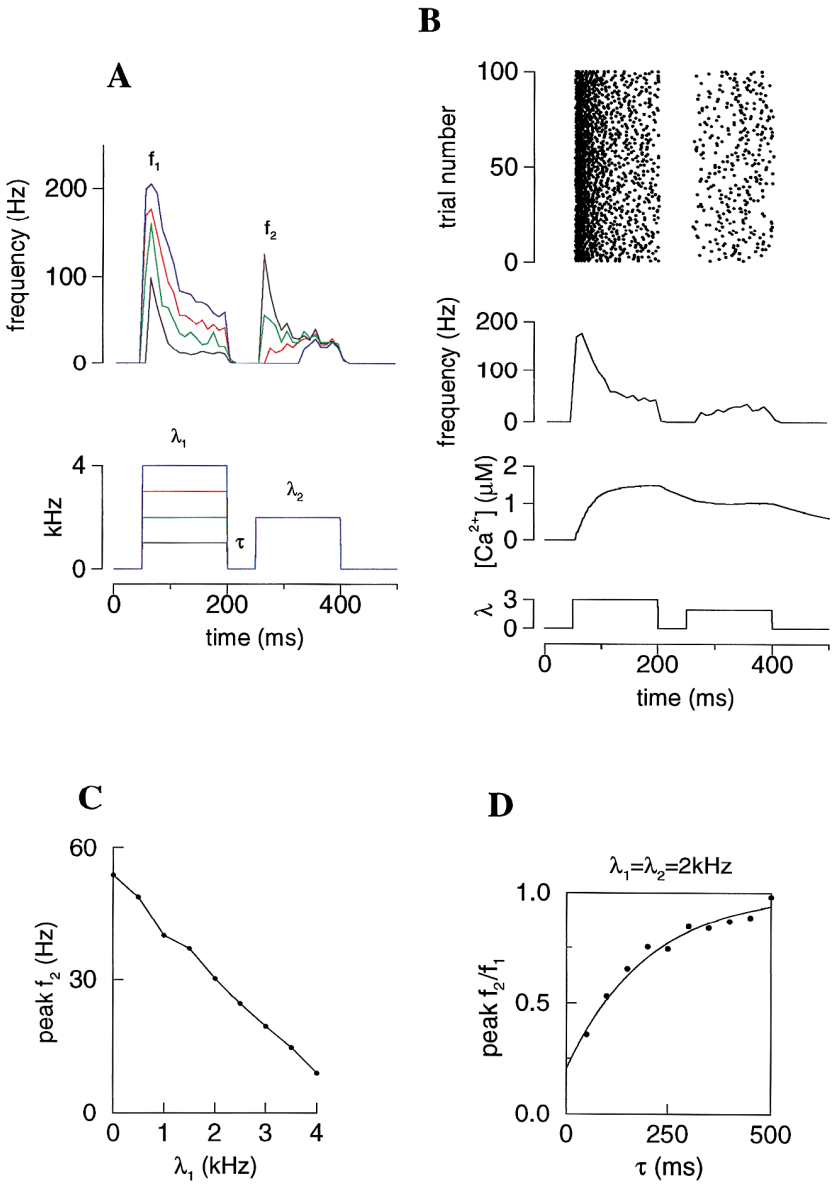

FIG. 12. Forward masking effect. *A*: 2 input pulses are presented to the cell model with a time separation of τ ms. With increasing amplitude of the first (masking) input, the response to the second (test) input is dramatically reduced. *B*: an example with the spike rastergram (*top*), the average instantaneous firing frequency (*middle top*). $[Ca^{2+}]$ does not have time to decay back to its baseline during the time interval between the masking and test pulses (*middle bottom*), this residual $[Ca^{2+}]$ is at the origin of the forward masking phenomenon. *C*: peak response to the test input is negatively proportional to the amplitude of the masking input. *D*: masking effect decreases with τ according to a recovery time course about exp $(-\tau/\tau_{Ca})$, τ_{Ca} = 200 ms. (Dendritic g_{AHP} = 6 mS/cm^2.)

''pops up'' in time. This represents a cellular selective attention mechanism operating in the temporal domain.

DISCUSSION

The main findings of this work are twofold and are summarized in the following text.

Quantitative theory of spike-frequency adaptation and calcium coding

Cortical neurons and networks display many forms of adaptation to sensory inputs. Here we focused on the spike-frequency adaptation and developed a method to predict its time course (in response to a current pulse) characterized by two quantities: the adaptation time constant τ_{adap} and the percentage adaptation F_{adap}. This procedure led to a reduction of the two-compartment conductance-based model to a simple calcium model of neuronal firing activity. It was shown that this calcium model can predict the instantaneous neuronal output as the input changes rapidly in time in an arbitrary manner partly because the effective time constant τ_{adap} for the $[Ca^{2+}]$ dynamics is much shorter than τ_{Ca} due to the adaptation feedback. This result confirms and strengthens the suggestion (Helmchen et al. 1996) that the intracellular Ca^{2+} is capable of encoding the temporal output computation of cortical pyramidal neurons. Of course, this description is limited to a rate code of neural information, the knowledge about the precise spike timing within a typical ISI being lost. Thus our calcium model is a firing-rate model of neuronal activity that is derived from a conductance-based model and that incorporates the spike-frequency adaptation, a main firing characteristic of regular spiking cortical pyramidal neurons.

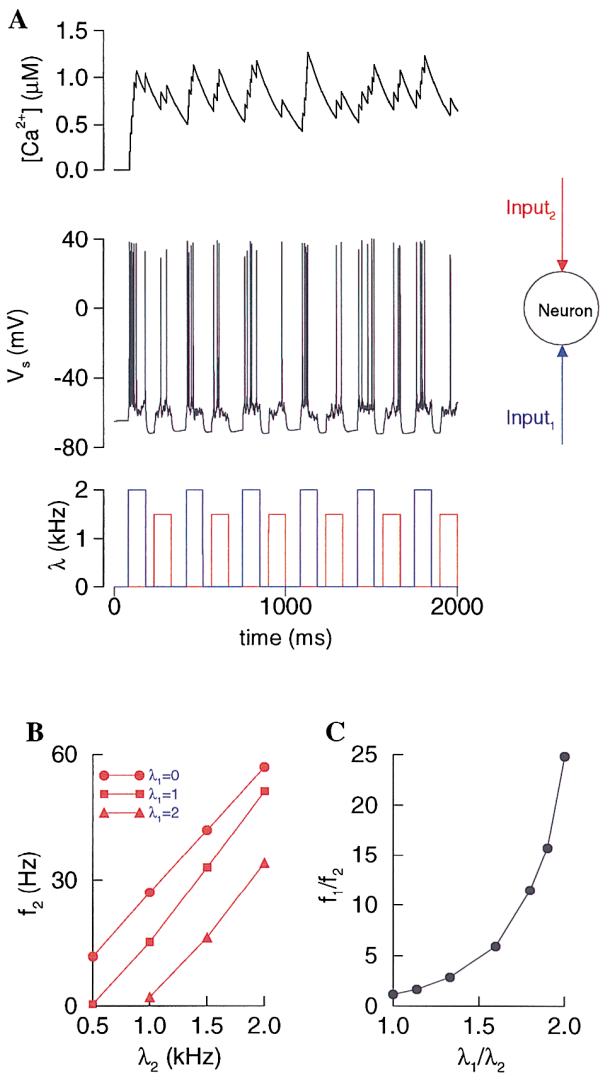

FIG. 13. Cellular selective attention. *A*: 2 input pulse trains (*blue* and *red*) are presented to the cell model with slightly different amplitudes (λ_1 and λ_2, respectively). Response to the weaker input f_2 is suppressed differentially as compared with f_1 to the stronger input. *B*: f_2 as function of λ_2, for 3 different λ_1 values. Presence of the masking input λ_1 shifts the *f-I* curve to the right but does not change the input-output slope. *C*: response ratio f_1/f_2 is a highly nonlinear function of the input ratio λ_1/λ_2, demonstrating a selective inhibition of the response to the weaker input. Dendritic $g_{AHP} = 6$ mS/cm^2, $\tau_{Ca} = 200$ ms.

Such a calcium-based model can be generalized to a network of interconnected pyramidal neurons.

Our analysis permitted us to derive τ_{adap} and F_{adap} in terms of the biophysical parameters of the membrane and intracellular Ca^{2+} dynamics. With plausible approximations, two relations between τ_{adap} and F_{adap} were obtained. The first relation is given by *Eq. 18*: $F_{adap} \simeq \alpha G_{cc} \tau_{adap}$, where αG_{cc} is a ''negative feedback gain parameter'' and is proportional to g_{Ca} and g_{AHP} but independent of all $[Ca^{2+}]$ extrusion and buffering processes. The second relation is given by *Eq. 19*: $F_{adap} \simeq 1 - \tau_{adap}/\tau_{Ca}$, which predicts a negative proportionality between the two quantities as long as τ_{Ca} is maintained fixed. We emphasize that these relations are not exact but only approximate (see Fig. 6). They are not expected to hold if the linear theory is not valid and the adaptation time course is not exponential, for example, when adaptation is so strong that the firing is blocked completely in the steady state (Guckenheimer et al. 1997; Madison and Nicoll 1984). Moreover, it is important to assess how these predictions depend on details of the model. We performed some limited computer simulations to address this tissue, using a different functional form for $I_{AHP} = g_{AHP}([Ca^{2+}]/([Ca^{2+}] + K_D)^q \times (V - E_K)$, with $q = 2$ (Koch et al. 1995) or $q = 3$ (Lytton and Sejnowski 1993; Zhang et al. 1995) instead of $q = 1$. In this case, the reduced calcium equation was no longer linear. Numerically, we found that the second relation between τ_{adap} and F_{adap} still held roughly with the slope comparable with, but larger than, $1/\tau_{Ca}$. Another issue concerned other ionic currents such as the $[Ca^{2+}]$-independent I_M (Madison and Nicoll 1984) or/and the nonspecific cation I_H (Lorenzon and Foehring 1992), which in some pyramidal neurons contribute to spike-frequency adaptation although to a much lesser extent than I_{AHP}. In principle, their effects could be analyzed in the same way as we did for I_{AHP}; the predicted relations between τ_{adap} and F_{adap} would need to be modified accordingly.

To the first order of approximation, however, we feel that the two relations are useful predictions that can be tested experimentally. The second relation can be assessed in pyramidal neurons, e.g., by measuring τ_{adap} and F_{adap} while a current pulse is applied with different intensities or when the g_{AHP} is blocked pharmacologically at various drug concentrations. These manipulations preserve τ_{Ca}, and our theory predicts that F_{adap} and τ_{adap} vary in such a way that they satisfy $F_{adap} \simeq 1 - \tau_{adap}/\tau_{Ca}$. Such measurements should provide an independent (if only crude) estimate for the $[Ca^{2+}]$ decay time τ_{Ca}. Furthermore, because g_{AHP} is known to be modulated by transmitters such as acetylcholine, norepinephrine, serotonin, and histamine (McCormick and Williamson 1989; Nicoll 1988; Pedarizani and Storm 1993), one can ask if neuromodulation of the g_{AHP} could strongly regulate the spike-frequency adaptation dynamics while preserving the simple relation between τ_{adap} and F_{adap}.

In addition, these relations could be used to assess how the biophysical mechanism for spike-frequency adaptation differs from cell to cell in neocortical circuits. Ahmed et al. (1993, 1997) have quantitatively described spike-frequency adaptation in in vivo pyramidal neurons of the cat primary visual cortex. It was found that there was a conspicuous difference between superficial and deep layer neurons: superficial layer cells adapt faster and more strongly ($\tau_{adap} = 11.5 \pm 1.3$ ms, and $F_{adap} = 67 \pm 3\%$) than deep layer cells ($\tau_{adap} = 51.4 \pm 6.4$ ms and $F_{adap} = 51 \pm 5\%$). According to our theoretical results, this finding cannot be explained primarily by a difference in the $[Ca^{2+}]$ extrusion/buffering processes between superficial and deep layer neurons. If that was the case, the relation $F_{adap} \simeq \alpha G_{cc} \tau_{adap}$ would predict that a smaller τ_{adap} should be correlated with a smaller F_{adap}, contrary to the observations.

Cellular selective attention and decorrelation

We investigated in detail the effect of spike-frequency adaptation to stochastic synaptic inputs of the Poisson type.

In particular, we showed that the $[Ca^{2+}]$-gated I_{AHP} can produce a forward masking effect similar to that shown experimentally in the Omega auditory neurons of the cricket (Sobel and Tank 1994). Essentially, the I_{AHP} provides a delayed negative feedback that is intrinsic to single pyramidal neurons and hence can be viewed as a cellular mechanism of lateral inhibition in time. Thus when two (or more) competing inputs converge onto a pyramidal neuron, the I_{AHP} can differentially suppress the responses to all but the strongest input (Fig. 13).

Because awake states are associated with activation of the brain stem cholinergic system and acetylcholine is a potent inhibitor of the I_{AHP} (and I_M) (McCormick and Williamsson 1989; Nicoll 1988), it is important to know how strong the spike-frequency adaptation effect is in pyramidal neurons during awake behavioral conditions. This question can be addressed, if the degree of neuronal adaptation can be assessed directly from extracellularly recorded spike trains. We found that the spike-frequency adaptation mechanism was manifested by a large negative coefficient of correlations of the ISIs (CC) (Figs. 8 and 9). Because the CC is readily computable from spike trains, it may subserve a probe for assessing the strength of adaptating ion currents (especially the I_{AHP}), under different in vivo conditions of the intact brain. Note that the CC is computed in the stationary state after transients. Therefore, in contrast to constant current pulses, with stochastic synaptic inputs the I_{AHP} is operative all the time and is responsible for generating negative temporal correlations between output ISIs in a frequency-dependent manner, whereas the Poisson input is totally uncorrelated in time. This result suggests that, if the inputs actually are correlated strongly in time, such positive correlations can be reduced (inputs are decorrelated) by a subtraction mechanism through spike-frequency adaptation. Computational implications of this observation will be explored in a separate work.

APPENDIX A: ISI RETURN MAP AND COEFFICIENT OF CORRELATION

For a neuronal spike train converted into a sequence of ISIs $\{t_1, t_2, t_3, \ldots, t_N\}$ (with a mean μ), the coefficient of correlation between consecutive ISIs (CC) is defined in *Eq. 7* of METHODS. Here we show that the CC is the same as the slope of the conditional average $\langle t_{n+1}|t_n\rangle$ versus t_n. Let $p(t_{n+1}, t_n)$ be the joint probability for t_{n+1} and t_n. Then by definition

$$\langle (t_{n+1} - \mu)(t_n - \mu)\rangle = \iint dt_{n+1}dt_n(t_{n+1} - \mu)(t_n - \mu)p(t_{n+1}, t_n) \quad (A1)$$

We can write $p(t_{n+1}, t_n) = p(t_n)p(t_{n+1}|t_n)$, where $p(t_{n+1}|t_n)$ is the conditional probability for t_{n+1} given t_n. Suppose that the conditional average of t_{n+1} given a fixed t_n is linear with t_n (for examples, see Figs. 8*C* and 11*B*)

$$\langle t_{n+1}|t_n\rangle = \int t_{n+1}p(t_{n+1}|t_n)dt_{n+1} \simeq \kappa t_n + \kappa_0 \quad (A2)$$

where κ is the slope and κ_0 is a constant. Then

$$\langle (t_{n+1} - \mu)(t_n - \mu)\rangle$$

$$= \int dt_n(t_n - \mu)p(t_n)\left(\int dt_{n+1}(t_{n+1} - \mu)p(t_{n+1}|t_n)_{+1}\right)$$

$$= \int dt_n(\langle t_{n+1}|t_n\rangle - \mu)(t_n - \mu)p(t_n)$$

$$\simeq \kappa \int dt_n(t_n - \mu)^2 p(t_n) = \kappa\sigma^2 \quad (A3)$$

Therefore, CC = κ. In other words, if the conditional average of t_{n+1} is plotted as function of its preceding value t_n, the slope κ is identical to the ISI coefficient of correlation.

APPENDIX B: DERIVATION OF SPIKE-FREQUENCY ADAPTATION TIME COURSE

The method is outlined in RESULTS. Here, we describe the procedure step by step. In *step 1*, we focus on the fast membrane dynamics *Eqs. 1–3*, where $[Ca^{2+}]$ is considered as a parameter rather than a variable. For a constant $[Ca^{2+}]$, the $I_{AHP} = g_{AHP}[[Ca^{2+}]/([Ca^{2+}] + K_D)](V - E_K)$ is a ''passive'' outward current. Given I, the larger is $[Ca^{2+}]$, so is I_{AHP}, and the less the neuron should fire. We simulated the membrane *Eqs. 1–3* with different $[Ca^{2+}]$ values. For each $[Ca^{2+}]$ value, the firing rate f was computed as well as the average $\langle I_{Ca}\rangle$ over an ISI; they are plotted in Fig. 2, *B* and *C*, respectively. These curves are nonlinear, in fact $f = 0$ for $[Ca^{2+}] > 2.2$ μM. However, if we restrict ourselves to the range of $[Ca^{2+}]$ between 0 and $[Ca^{2+}]_{ss} = 1.74$ μM of Fig. 2*A*, the two curves in Fig. 2, *B* and *C*, can be approximated well by straight lines. This yields

$$f \simeq f_0 - G_f[Ca^{2+}] \quad \langle I_{Ca}\rangle \simeq \langle I_{Ca}\rangle_0 + G_{cc}[Ca^{2+}] \quad (B1)$$

with $f_0 = 271$, $G_f = 84$, $\langle I_{Ca}\rangle_0 = -28.8$, and $G_{cc} = 10$ (Fig. 2, *B* and *C*, *red solid lines*).

In *step 2*, we turn our attention to the slowly evolving dynamics of $[Ca^{2+}]$, *Eq. 4*. Because $[Ca^{2+}]$ varies slowly, we substitute I_{Ca} by its average $\langle I_{Ca}\rangle$ which is a function of $[Ca^{2+}]$ itself (*Eq. B1*). Therefore, we have

$$\begin{aligned}\frac{d[Ca^{2+}]}{dt} &\simeq -\alpha\langle I_{Ca}\rangle - [Ca^{2+}]/\tau_{Ca}\\ &= -\alpha(\langle I_{Ca}\rangle_0 + G_{cc}[Ca^{2+}]) - [Ca^{2+}]/\tau_{Ca}\\ &= -\alpha\langle I_{Ca}\rangle_0 - (\alpha G_{cc} + 1/\tau_{Ca})[Ca^{2+}]\\ &= -\alpha\langle I_{Ca}\rangle_0 - [Ca^{2+}]/\tau_{adap} \quad (B2)\end{aligned}$$

with

$$\frac{1}{\tau_{adap}} = \alpha G_{cc} + \frac{1}{\tau_{Ca}} \quad (B3)$$

Solving the averaged equation, we have

$$[Ca^{2+}](t) = [Ca^{2+}]_{ss}(1 - \exp(-t/\tau_{adap})),$$

$$\text{with} \quad [Ca^{2+}]_{ss} = -\alpha\langle I_{Ca}\rangle_0\tau_{adap} \quad (B4)$$

Using the numerical values of the parameters in this expression, we obtain $[Ca^{2+}]_{ss} = 1.77$ μM and $\tau_{adap} = 30.8$ ms. These predicted values are close to those from numerical simulations of the whole model system ($[Ca^{2+}]_{ss} = 1.74$ μM, $\tau_{adap} = 33$ ms, respectively). Finally, in *step 3*, we insert the time course for $[Ca^{2+}]$ into the expression $f = f_0 - G_f[Ca^{2+}]$, which yields

$$\begin{aligned}f(t) &= f_0 - G_f[Ca^{2+}](t) = f_0 - G_f[Ca^{2+}]_{ss}(1 - \exp(-t/\tau_{adap}))\\ &= f_0 - G_f[Ca^{2+}]_{ss} + G_f[Ca^{2+}]_{ss}\exp(-t/\tau_{adap})\\ &= f_{ss} + (f_0 - f_{ss})\exp(-t/\tau_{adap}) \quad (B5)\end{aligned}$$

where $f_{ss} = f_0 - G_f[Ca^{2+}]_{ss}$. Using the numerical values for f_0 and G_f, we obtain $f_0 = 271$ Hz and $f_{ss} = 122$ Hz, compared with numerical values of $f_0 = 272$ Hz and $f_{ss} = 116$ Hz. The slight

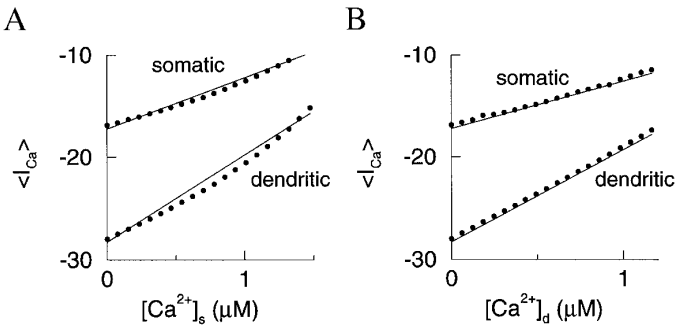

FIG. B1. Average firing rate f, $\langle I_{Ca,s} \rangle$ and $\langle / I_{Ca,d} \rangle$ as functions of $[Ca^{2+}]_s$ *(A)* and $[Ca^{2+}]_d$ *(B)* for the fast-slow variable analysis. ——, linear approximations.

overestimate of f_{ss} is due to a small nonlinearity of the f-$[Ca^{2+}]$ curve (Fig. 2*B*).

APPENDIX C: ADAPTATION TIME CONSTANTS BY TWO COUPLED CALCIUM MODES

With I_{Ca} and I_{AHP} in both somatic and dendritic compartments, we attempted to generalize our fast-slow variable analysis to predict the biphasic spike-frequency adaptation time course. In *step 1*, we hold $[Ca^{2+}]_s$ and $[Ca^{2+}]_d$ as parameters. We make the simple assumption that the two adapting currents act independently and additively, so we numerically compute the dependence of the firing rate f and the calcium currents $I_{Ca,s}$ and $I_{Ca,d}$ on each of the $[Ca^{2+}]_s$ and $[Ca^{2+}]_d$ separately. For instance, if we consider the effect of the somatic I_{AHP} on spike-frequency adaptation, we let $[Ca^{2+}]_d = 0$ while $[Ca^{2+}]_s$ is varied, we have (Fig. B1*A*)

$$f = f_0 - G_{f,s}[Ca^{2+}]_s$$
$$\langle I_{Ca,s} \rangle = \langle I_{Ca,s} \rangle_0 + G_{cc,ss}[Ca^{2+}]_s$$
$$\langle I_{Ca,d} \rangle = \langle I_{Ca,d} \rangle_0 + G_{cc,ds}[Ca^{2+}]_s \quad (C1)$$

with $f_0 = 272$, $\langle I_{Ca,s} \rangle_0 = -17.2$, $\langle I_{Ca,d} \rangle_0 = -28.3$, $G_{f,d} = 81.4$, $G_{cc,ss} = 5$, and $G_{cc,ds} = 8.5$.

On the other hand, the effect of the dendritic I_{AHP} is considered with $[Ca^{2+}]_s = 0$ while $[Ca^{2+}]_d$ is varied as parameter, we have (Fig. B1*B*)

$$f = f_0 - G_{f,d}[Ca^{2+}]_d$$
$$\langle I_{Ca,s} \rangle = \langle I_{Ca,s} \rangle_0 + G_{cc,sd}[Ca^{2+}]_d$$
$$\langle I_{Ca,d} \rangle = \langle I_{Ca,d} \rangle_0 + G_{cc,dd}[Ca^{2+}]_d \quad (C2)$$

with $G_{f,d} = 75$, $G_{cc,sd} = 4.6$, and $G_{cc,dd} = 9$.

The combined effect of both $I_{AHP,s}$ and $I_{AHP,d}$ is expressed as

$$f = f_0 - G_{f,s}[Ca^{2+}]_s - G_{f,d}[Ca^{2+}]_d$$
$$\langle I_{Ca,s} \rangle = \langle I_{Ca,s} \rangle_0 + G_{cc,ss}[Ca^{2+}]_s + G_{cc,sd}[Ca^{2+}]_d$$
$$\langle I_{Ca,d} \rangle = \langle I_{Ca,d} \rangle_0 + G_{cc,ds}[Ca^{2+}]_s + G_{cc,dd}[Ca^{2+}]_d \quad (C3)$$

In *step 2*, we substitute $I_{Ca,s}$ and $I_{Ca,d}$ by their averages *Eq. C3*, which yields two-coupled linear equations

$$\frac{d[Ca^{2+}]_s}{dt} = A_{c,s} - B_{ss}[Ca^{2+}]_s - B_{sd}[Ca^{2+}]_d$$
$$\frac{d[Ca^{2+}]_d}{dt} = A_{c,d} - B_{ds}[Ca^{2+}]_s - B_{dd}[Ca^{2+}]_d \quad (C4)$$

where $A_{c,s} = -\alpha_s \langle I_{Ca,s} \rangle_0$, $A_{c,d} = -\alpha_d \langle I_{Ca,d} \rangle_0$; $B_{ss} = \alpha_s G_{cc,ss} + 1/\tau_{Ca,s}$, $B_{sd} = \alpha_s G_{cc,sd}$, $B_{ds} = \alpha_d G_{cc,ds}$, $B_{dd} = \alpha_d G_{cc,dd} + 1/\tau_{Ca,d}$.

The solution of *Eq. C4* has the form

$$[Ca^{2+}]_s(t) = [Ca^{2+}]_{s,ss} + c_{s1} \exp(-t/\tau_{adap,1}) + c_{s2} \exp(-t/\tau_{adap,2})$$
$$[Ca^{2+}]_d(t) = [Ca^{2+}]_{d,ss} + c_{d1} \exp(-t/\tau_{adap,1}) + c_{d2} \exp(-t/\tau_{adap,2}) \quad (C5)$$

where the time constants are given by the eigenvalues of the matrix

$$-\begin{pmatrix} B_{ss} & B_{sd} \\ B_{ds} & B_{dd} \end{pmatrix} \quad (C6)$$

Explicit calculations yield $\tau_{adap,1} = 30.7$ ms and $\tau_{adap,2} = 184$ ms. And solving *Eq. C4* we have $[Ca^{2+}]_{s,ss} = 1.0$, $c_{s1} = -0.22$, $c_{s2} = -0.77$, $[Ca^{2+}]_{d,ss} = 1.3$, $c_{d1} = -1.8$, $c_{d2} = +0.52$ (in μM).

The fact that c_{d1} and c_{d2} have different signs implies that the time course $[Ca^{2+}]_d(t)$ is not monotonic and exhibits a maximum. Indeed, we can find the time t_{max} when the maximum occurs by letting $d[Ca^{2+}]_d/dt = 0$, which yields

$$-\frac{c_{d1}}{\tau_{adap,1}} \exp(-t_{max}/\tau_{adap,1}) - \frac{c_{d2}}{\tau_{adap,2}} \exp(-t_{max}/\tau_{adap,2}) = 0 \quad (C7)$$

or, solving this algebraic equation,

$$t_{max} = \frac{\tau_{adap,1}\tau_{adap,2}}{\tau_{adap,2} - \tau_{adap,1}} \ln\left(\frac{-c_{d1}\tau_{adap,2}}{c_{d2}\tau_{adap,1}}\right) = 112 \text{ ms} \quad (C8)$$

which compared well with the numerical value of the peak time (= 106 ms).

Finally, in *step 3*, by inserting the solutions for $[Ca^{2+}]_s(t)$ and $[Ca^{2+}]_d(t)$ into the expression of the firing rate (*Eq. C3*), we obtain

$$f(t) = f_{ss} + b_1 \exp(-t/\tau_{adap,1}) + b_2 \exp(-t/\tau_{adap,2}) \quad (C9)$$

with $f_{ss} = 93$, $b_1 = 153.6$, $b_2 = 23.7$ (in Hz).

Compared with the empirical fits given by *Eq. 21*, we see that the linear theory predicts reasonably well the two adaptation time constants but not the steady-state values and the weighting factors for the two modes (the coefficients in *Eqs. C5* and *C9*). We found that the linear analysis is not accurate, because there are significant interactions between the two modes which would introduce cross-product terms like $[Ca^{2+}]_s \times [Ca^{2+}]_d$ in *Eq. C3*. An improved nonlinear analysis is beyond the scope of this paper.

I thank G. Turrigiano for comments on the manuscript.

This work was supported by National Institute of Mental Health Grant MH-53717-01), the Alfred P. Sloan Foundation, and the W. M. Keck Foundation.

Address reprint requests to X.-J. Wang.

Received 8 July 1997; accepted in final form 3 December 1997.

REFERENCES

AGIN, D. Hodgkin-Huxley equations: logarithmic relation between membrane current and frequency of repetitive activity. *Nature* 201: 625–626, 1964.

AHMED, B., ANDERSON, C., DOUGLAS, R. J., AND MARTIN, K.A.C. A method of estimating net somatic input current from the action potential discharge of neurones in the visual cortex of the anaesthetised cat. (Abstract). *J. Physiol. (Lond.)* 459: 134, 1993.

AVOLI, M., HWA, G.G.C., LACAILLE, J.-C., OLIVIER, A., AND VILLEMURE, J. G. Electrophysiological and repetitive firing properties of neurons in the superficial/middle layers of the human neocortex maintained in vitro. *Exp. Brain Res.* 98: 135–144, 1994.

BAER, S. M., RINZEL, J., AND CARRILLO, H. Analysis of an autonomous phase model for neuronal parabolic bursting. *J. Math. Biol.* 33: 309–333, 1995.

BARKAI, E. AND HASSELMO, M. E. Modulation of the input-output function of rat piriform cortex pyramidal cells. *J. Neurophysiol.* 72: 644–658, 1994.

BALDISSERA, F. AND GUSTAFSSON, B. Firing behaviour of a neurone model based on the afterhyperpolarization conductance time course and algebraical summation. Adaptation and steady state firing. *Acta Physiol. Scand.* 92: 27–47, 1974.

BERNANDER, Ö, KOCH, C., AND DOUGLAS, R. J. Amplification and linearization of distal synaptic input to cortical pyramidal cells. *J. Neurophysiol.* 72: 2743–2753, 1994.

CONNORS, B. W., GUTNICK, M. J., AND PRINCE, D. A. Electrophysiological properties of neocortical neurons in vitro. *J. Neurophysiol.* 48: 1302–1320, 1982.

CROOK, S., ERMENTROUT, G. B., VANIER, M. C., AND BOWER, J. M. The role of axonal delay in the synchronization of networks of coupled cortical oscillators. *J. Comput. Neurosci.* 4: 161–172, 1997.

DOUGLAS, R. J., KOCH, C., MAHOWALD, M., MARTIN, K.A.C., AND SUAREZ, H. H. Recurrent excitation in neocortical circuits. *Science* 269: 981–985, 1995.

ERMENTROUT, G. B. Reduction of conductance-based models with slow synapses to neural nets. *Neural Comput.* 6: 679–695, 1994.

FOEHRING, R., LORENZON, N. M., HERRON, P., AND WILSON, C. J. Correlation of physiologically and morphologically identified neuronal types in human association cortex in vitro. *J. Neurophysiol.* 65: 1825–1837, 1991.

GUCKENHEIMER, J., HARRIS-WARRICK, R., PECK, J., AND WILLMS, A. Bifurcation, bursting, and spike frequency adaptation. *J. Comput. Neurosci.* 4: 257–277, 1997.

GUSTAFSSON, B. AND WIGSTRÖM, H. Shape of frequency-current curves in CA1 pyramidal cells in the hippocampus. *Brain Res.* 223: 417–421, 1981.

HELMCHEN, F., IMOTO, K., AND SAKMANN, B. Ca^{2+} buffering and action potential-evoked Ca^{2+} signaling in dendrites of pyramidal neurons. *Biophys. J.* 70: 1069–1081, 1996.

HODGKIN, A. L. AND HUXLEY, A. F. A quantitative description of membrane current and its application to conduction and excitation in nerve. *J. Physiol. (Lond.)* 117: 500–544, 1952.

HOFFMAN, D. A., MAGEE, J. C., COLBERT, C. M., AND JOHNSTON, D. K^+ channel regulation of signal propagation in dendrites of hippocampal pyramidal neurons. *Nature* 387: 869–875, 1997.

HOTSON, J. R. AND PRINCE, D. A. A calcium-activated hyperpolarization follows repetitive firing in hippocampal neurons. *J. Neurophysiol.* 43: 409–419, 1980.

JAFFE, D. B., ROSS, W. N., LISMAN, J. E., LASSER-ROSS, N., MIYAKAWA, H., AND JOHNSTON, D. A model for dendritic Ca^{2+} accumulation in hippocampal pyramidal neurons based on fluorescence imagining measurements. *J. Neurophysiol.* 71: 1065–1077, 1994.

JOHNSTON, D. The calcium code. *Biophys. J.* 70: 1095, 1996.

JOHNSTON, D., MAGEE, J. C., COLBERT, C. M., AND CHRISTIE, B. R. Active properties of neuronal dendrites. *Annu. Rev. Neurosci.* 19: 165–186, 1996.

KAY, A. R. AND WONG, R.K.S. Calcium current activation kinetics in isolated pyramidal neurones of the CA1 region of the mature guinea-pig hippocampus. *J. Physiol. (Lond.)* 392: 603–616, 1987.

KIM, H. G. AND CONNORS, E. W. Apical dendrites of the neocortex: correlation between sodium- and calcium-dependent spiking and pyramidal cell morphology. *J. Neurosci.* 13: 5301–5311, 1993.

KOCH, C., BERNANDER, Ö., AND DOUGLAS, R. J. Do neurons have a voltage or a current threshold for action potential initiation? *J. Comput. Neurosci.* 2: 63–82, 1995.

LANCASTER, B. AND ADAMS, P. R. Calcium-dependent current generating the afterhyperpolarization of hippocampal neurons. *J. Neurophysiol.* 55: 1268–1282, 1986.

LANCASTER, B. AND ZUCKER, R. S. Photolytic manipulation of Ca^{2+} and the time course of slow, Ca^{2+}-activated K^+ current in rat hippocampal neurones. *J. Physiol. (Lond.)* 475: 229–239, 1994.

LANTHORN, T., STORM, J. AND ANDERSEN, P. Current-to-frequency transduction in CA1 hippocampal pyramidal cells: slow prepotentials dominate the primary range firing. *Exp. Brain Res.* 53: 431–443, 1984.

LLINÁS, R. R. The intrinsic electrophysiological properties of mammalian neurons: insights into central nervous system function. *Science* 242: 1654–1664, 1988.

LORENZON, N. M. AND FOEHRING, R. C. Relationship between repetitive firing and afterhyperpolarizations in human neocortical neurons. *J. Neurophysiol.* 67: 350–363, 1992.

LYTTON, W. W. AND SEJNOWSKI, T. J. Simulations of cortical pyramidal neurons synchronized by inhibitory interneurons. *J. Neurophysiol.* 66: 1059–1079, 1991.

MADISON, D. V., LANCASTER, B., AND NICOLL, R. A. Voltage clamp analysis of cholinergic action in the hippocampus. *J. Neurosci.* 7: 733–741, 1987.

MADISON, D. V. AND NICOLL, R. A. Control of the repetitive discharge of rat CA1 pyramidal neurons *in vitro. J. Physiol. (Lond.)* 354: 319–331, 1984.

MAINEN, Z. F. AND SEJNOWSKI, T. J. Influence of dendritic structure on firing pattern in model neocortical neurons. *Nature* 382: 363–366, 1996.

MARDER, E., ABBOTT, L., TURRIGIANO, G., LIU, Z., AND GOLOWASH, J. Memory from the dynamics of intrinsic membrane currents. *Proc. Natl. Acad. Sci. USA* 93: 13482–13486, 1996.

MARKRAM, H., HELM, P. J., AND SAKMANN, B. Dendritic calcium transients evoked by single back-propagating action potentials in rat-neocortical pyramidal neurons. *J. Physiol. (Lond.)* 485: 1–20, 1995.

MASON, A. AND LARKMAN, A. Correlation between morphology and electrophysiology of pyramidal neurons in slices of rat visual cortex. II. electrophysiology. *J. Neurosci.* 10: 1415–1428, 1990.

MCCORMICK, D. A. AND WILLIAMSON, A. Convergence and divergence of neurotransmitter action in human cerebral cortex. *Proc. Natl. Acad. Sci. USA* 86: 8098–8102, 1989.

MCCORMICK, D. A., CONNORS, B. W., LIGHTHALL, J. W., AND PRINCE, D. A. Comparative electrophysiology of pyramidal and sparsely spiny stellate neurons of the neocortex. *J. Neurophysiol.* 54: 782–806, 1985.

MIYAKAWA, H., ROSS, W. N., JAFFE, D., CALLAWAY, J. C., LASSER-ROSS, N., LISMAN, J. E., AND JOHNSTON, D. Synaptically activated increases in Ca^{2+} concentration in hippocampal CA1 pyramidal cells are primarily due to voltage-gated Ca^{2+} channels. *Neuron* 9: 1163–1173, 1992.

NICOLL, R. A. The coupling of neurotransmitter receptors to ion channels in the brain. *Science* 241: 545–551, 1988.

NISHIMURA, Y., KITAGAWA, H., SAITOH, K., ASAHI, M., ITOH, K., YOSHIOKA, K., ASAHARA, T., TANAKA, T., AND YAMAMOTO, T. The burst firing in the layer III and V pyramidal neurons of the cat sensorimotor cortex in vitro. *Brain Res.* 727: 212–216, 1996.

PERKEL, D. H., GERSTEIN, G. L., AND MOORE, G. P. Neuronal spike trains and stochastic point processes. I. The single spike train. *Biophys. J.* 7: 391–418, 1967.

PEDARZANI, P. AND STORM, J. F. PKA mediates the effects of monoamine transmitters on the K^+ current underlying the slow spike frequency adaptation in hippocampal neurons. *Neuron* 11: 1023–1035, 1993.

PINSKY, P. F. AND RINZEL, J. Intrinsic and network rhythmogenesis in a reduced Traub model for CA3 neurons. *J. Comput. Neurosci.* 1: 39–60, 1994.

POLLACK, G. S. Selective attention in an insect auditory neuron. *J. Neurosci.* 8: 2635–2639, 1988.

PRESS, W. H., FLANNERY, B. P., TEUKOLSKY, S. A., AND VETTERLING, W. T. *Numerical Recipes.* Cambridge: Cambridge University Press, 1989.

RHODES, P. A. AND GRAY, C. M. Simulation of intrinsically bursting neocortical pyramidal neurons. *Neural Comput.* 6: 1086–1110, 1994.

RINZEL, J. A formal classification of bursting mechanisms in excitable cells. In: *Proc. Int. Congress of Mathematicians*, edited by A. M. Glesson. Providence, RI: Am. Math. Soc., 1987, p. 1578–1594.

RINZEL, J. AND ERMENTROUT, G. B. In: *Methods in Neuronal Modeling*, edited by C. Koch and I. Segev. Cambridge, MA: MIT Press, 1989, p. 135–170.

RUDY, B. Diversity and ubiquity of K channels. *Neuroscience* 25: 729–749, 1988.

SCHILLER, J., HELMCHEN, F., AND SAKMANN, B. Spatial profile of dendrite calcium transients evoked by action potentials in rat neocortical pyramidal neurons. *J. Physiol. (Lond.)* 487: 583–600, 1995.

SCHWINDT, P. C., SPAIN, W. J., FOEHRING, R. C., STAFSTROM, C. E., CHUBB, M. C., AND CRILL, W. E. Multiple potassium conductances and their functions in neurons from cat sensorimotor cortex in vitro. *J. Neurophysiol.* 59: 424–449, 1988.

SOBEL, E. AND TANK, D. W. In vivo Ca^{2+} dynamics in a cricket auditory neuron: an example of chemical computation. *Science* 263: 823–826, 1994.

SOFTKY, W. R. AND KOCH, C. The highly irregular firing of cortical cells is inconsistent with temporal integration of random EPSPs. *J. Neurosci.* 13: 334–350, 1993.

STERN, R. B. A theoretical analysis of neuronal variability. *Biophys. J.* 5: 173–194, 1965.

STERN, E. A., KINCAID, A. E., AND WILSON, C. J. Spontaneous subthreshold membrane potential fluctuations and action potential variability of rat corticostriatal and striatal neurons in vivo. *J. Neurophysiol.* 77: 1697–1715, 1997.

STORM, J. F. Temporal integration by a slowly inactivating K^+ current in hippocampal neurons. *Nature* 336: 379–381, 1988.

STORM, J. F. Potassium currents in hippocampal pyramidal cells. *Prog. Brain Res.* 83: 161–187, 1990.

SVOBODA, K., DENK, W., KLEINFELD, D., AND TANK, D. In vivo dendritic calcium dynamics in neocortical pyramidal neurons. *Nature* 385: 161–165, 1997.

TANK, D. W., REGEHR, W. G., AND DELANEY, K. R. A quantitative analysis of presynaptic calcium dynamics that contribute to short-term enhancement. *J. Neurosci.* 15: 7940–7952, 1995.

TRAUB, R. D. Simulation of intrinsic bursting in CA3 hippocampal neurons. *Neuroscience* 7: 1233–1242, 1982.

TRAUB, R. D., JEFFERYS, J.G.R., MILES, R., WHITTINGTON, M. A., AND TÓTH, K. A branching dendritic model of a rodent CA3 pyramidal neurone. *J. Physiol. (Lond.)* 481: 79–95, 1994.

TUCKWELL, H. *Introduction to Theoretical Neurobiology*. Cambridge, UK: Cambridge University Press, 1988, vol. 2.

TURRIGIANO, G., MARDER, E., AND ABBOTT, L. F. cellular short-term memory from a slow potassium conductance. *J. Neurophysiol.* 75: 963–966, 1996.

WANG, X.-J. Ionic basis for intrinsic 40 Hz neuronal oscillations. *NeuroReport* 5: 221–224, 1993.

WANG, X.-J. AND RINZEL, J. Oscillatory and Bursting Properties of Neurons. In: *The Handbook of Brain Theory and Neural Networks*, edited by M. Arbib. Cambridge, MA: MIT Press, 1995, p. 686–691.

WILBUR, W. J. AND RINZEL, J. A theoretical basis for large coefficient of variation and bimodality in neuronal interspike interval distributions. *J. Theor. Biol.* 105: 345–368, 1983.

WILSON, C. J. Dynamic modification of dendritic cable properties and synaptic transmission by voltage-gated potassium channels. *J. Comput. Neurosci.* 2: 91–115.

YAMADA, W. M., KOCH, C., AND ADAMS, P. R. In: *Methods in Neuronal Modeling*, edited by C. Koch and I. Segev. Cambridge, MA: MIT Press, 1989, p. 97–134.

YUSTE, R. AND TANK, D. W. Dendritic integration in mammalian neurons, a century after Caja. *Neuron* 16: 701–716, 1996.

YUSTE, R., GUTNICK, M. J., SAAR, D., DELANEY, K. R., AND TANK, D. W. Ca+2 accumulations in dendrites of neocortical pyramidal neurons: an apical band and evidence for two functional compartments. *Neuron* 13: 23–43, 1994.

ZHANG, L., PENNEFATHER, P., VELUMIAN, A., TYMIANSKI, M., CHARLTON, M., AND CARLEN, P. L. Potentiation of a slow Ca^{2+}-dependent K^+ current by intracellular Ca^{2+} chelators in hippocampal CA1 neurons of rat brain slices. *J. Neurophysiol.* 74: 2225–2241, 1995.